

Learning Power Spectrum Maps from Quantized Power Measurements

Daniel Romero, *Member, IEEE*, Seung-Jun Kim, *Senior Member, IEEE*,
Georgios B. Giannakis, *Fellow, IEEE*, and Roberto López-Valcarce, *Member, IEEE*

Abstract—Using power measurements collected by a network of low-cost sensors, power spectral density (PSD) maps are constructed to capture the distribution of RF power across space and frequency. Linearly compressed and quantized power measurements enable wideband sensing at affordable implementation complexity using a small number of bits. Strengths of data- and model-driven approaches are combined to develop estimators capable of incorporating multiple forms of spectral and propagation prior information while fitting the rapid variations of shadow fading across space. To this end, novel nonparametric and semiparametric formulations are investigated. It is shown that the desired PSD maps can be obtained using support vector machine-type solvers. In addition to batch approaches, an online algorithm attuned to real-time operation is developed. Numerical tests assess the performance of the novel algorithms.

I. INTRODUCTION

Power spectral density (PSD) cartography relies on sensor measurements to map the radiofrequency (RF) signal power distribution over a geographical region. The maps obtained are instrumental for various wireless network management tasks, such as power control, interference mitigation, and planning [12], [21]. For instance, wireless network planning can benefit from PSD maps since the latter reveal the location of crowded areas and areas of weak coverage, thus suggesting where new base stations should be deployed. Because they characterize how RF power distributes per channel across space, PSD maps also come handy to increase frequency reuse and mitigate interference in cellular systems. In addition, PSD maps enable opportunistic transmission in cognitive radio systems by unveiling underutilized “white spaces” in time, space, and frequency [5], [41]. Different from spectrum sensing techniques that assume a common spectrum occupancy over the sensed

region [3], [25], [28], PSD cartography accounts also for the variability along the spatial dimensions, thus enabling a more aggressive spatial reuse.

Spatial interpolation of RF power measurements has so far been approached using Kriging [1], compressive sampling [19], sparse Bayesian models [18], dictionary learning [22], [23], and matrix completion [15]. The estimated maps describe how power distributes over space but not frequency. Relying on basis expansions over the frequency dimension, methods to estimate PSD maps from *PSD measurements* such as periodograms were also developed [6], [8], [13]. However, communicating periodograms to the fusion center may incur high overhead and energy consumption. Recently, a low-overhead sensing scheme based on single-bit data was considered by [25] along the lines of [29], but the PSD is assumed constant across space.

To summarize, existing spectrum cartography approaches either construct *power* maps from *power* measurements, or, *PSD* maps from *PSD* measurements. In contrast, the main contribution of this paper is to present algorithms capable of estimating *PSD* maps from *power* measurements, thus attaining a more efficient extraction of the information contained in the observations than existing methods. Therefore, the proposed approach enables estimation of the RF power distribution over *frequency and space* using low-cost low-power sensors since only power measurements are required. Towards facilitating practical implementations with sensor networks, where communication bandwidth is limited, two measures are adopted to reduce overhead. First, sensor measurements are quantized to a small number of bits. Second, available prior information is efficiently captured both in the frequency and spatial domains, thus affording stronger quantization while minimally sacrificing the quality of the map estimate.

Specifically, a great deal of frequency-domain prior information about impinging communication waveforms can be gleaned from spectrum regulations and standards, which specify bandwidth, carrier frequencies, transmission masks, roll-off factors, number of sub-carriers, and so forth [30], [37]. To accommodate this information, a basis expansion model is adopted. Estimates of the power of each sub-channel and background noise can be obtained as a byproduct of adopting such an expansion. These estimates can be employed to construct signal-to-noise ratio (SNR) maps, which reveal weak coverage areas. Moreover, the aforementioned noise power estimates alleviate the well-known noise uncertainty problem in cognitive radio [35].

To incorporate varying degrees of prior information along the spatial dimensions, nonparametric and semiparametric regres-

D. Romero and R. López-Valcarce were supported by the European Regional Development Fund (ERDF) and the Spanish Government (TEC2010-21245-C02-02/TCM DYNACS, CONSOLIDER-INGENIO 2010 CSD2008-00010 COMONSENS), FPU Grant AP2010-0149, and the Galician Regional Government (CN 2012/260 AtlantTIC). D. Romero and G. B. Giannakis were supported by ARO grant W911NF-15-1-0492 and NSF grant 1343248. S.-J. Kim was supported by NSF grant 1547347.

D. Romero and G. B. Giannakis are with the Dept. of ECE and the Digital Tech. Center, Univ. of Minnesota, USA. E-mails: {dromero,georgios}@umn.edu. S.-J. Kim is with the Dept. of Computer Sci. & Electrical Eng., Univ. of Maryland, Baltimore County, USA. E-mail: sjkim@umbc.edu. R. López-Valcarce is with the Dept. of Signal Theory and Communications, Univ. of Vigo, Spain. E-mail: valcarce@gts.uvigo.es.

Parts of this work have been presented at the IEEE International Conference on Acoustics, Speech, and Signal Processing, Brisbane (Australia), 2015; at the Conference on Information Sciences and Systems, Baltimore (Maryland), 2015; and at the IEEE International Workshop on Computational Advances in Multi-sensor Adaptive Processing, Cancun (Mexico), 2015.

sion techniques are developed. The former pursue estimates that minimize appropriate regularization criteria over reproducing kernel Hilbert spaces (RKHS) of vector-valued functions [26]. Such estimates are useful when no prior knowledge about the propagation environment is available since they can approximate any RF power spatial distribution with arbitrarily high accuracy [11]. In many cases, however, one may approximately know the transmitter locations, the path loss exponent, or even the locations of obstacles or reflectors. To accommodate these sorts of prior information, a basis expansion is introduced and the theory of regression in RKHSs of vector-valued functions is extended to develop semiparametric estimators. This approach generalizes thin-plate spline regression [39], whose merits in spectrum cartography are well appreciated [8], to operate on quantized measurements. Moreover, the proposed semiparametric regression method for vector-valued functions is of independent interest since it can be applied beyond the present spectrum cartography context to estimate vector fields using sensor networks.

State-of-the-art statistical learning tools are adapted to gain robustness to measurement errors. In this sense, one major contribution of this work is a neat link between function estimation using quantized observations and support vector machines (SVMs) [31], [33], [34]. This link endows the proposed estimators with the universality of SVMs and provides useful guidelines to solve the resulting optimization problems.

Although the novel estimators can be implemented through efficient batch algorithms, limited computational resources may hinder real-time operation if an extensive set of measurements is to be processed. To mitigate this issue, an online nonparametric estimation algorithm is also developed based on stochastic gradient descent in RKHSs. The proposed algorithm defeats the curse of kernelization [40], and can also be applied to the general setup of kernel-based vector field estimation.

The rest of the paper is organized as follows. The system model and the problem statement are presented in Sec. II. The map estimation algorithms are presented in Sec. III. The online solver is developed in Sec. IV, while the numerical tests are the subject of Sec. V. Conclusions are drawn in Sec. VI.

Notation. The cardinality of set \mathcal{A} is denoted by $|\mathcal{A}|$. Scalars are denoted by lowercase letters, and matrices by bold uppercases. Superscript T stands for transposition, and H for conjugate transposition. The (i, j) th entry (j th column) of matrix \mathbf{A} is denoted by $a_{i,j}$ (\mathbf{a}_j). Symbol \otimes represents the Kronecker product, and \odot the Khatri-Rao product; that is, for $\mathbf{A} := [\mathbf{a}_1, \mathbf{a}_2, \dots, \mathbf{a}_N] \in \mathbb{C}^{M_1 \times N}$ and $\mathbf{B} := [\mathbf{b}_1, \mathbf{b}_2, \dots, \mathbf{b}_N] \in \mathbb{C}^{M_2 \times N}$, $\mathbf{A} \otimes \mathbf{B} = [\mathbf{a}_1 \otimes \mathbf{b}_1, \dots, \mathbf{a}_N \otimes \mathbf{b}_N] \in \mathbb{C}^{M_1 M_2 \times N}$. The Hadamard product $\mathbf{A} \circ \mathbf{B}$ is the entry-wise product: $(\mathbf{A} \circ \mathbf{B})_{i,j} = a_{i,j} b_{i,j}$. Vector $\mathbf{e}_{M,i}$ is the i -th canonical basis of \mathbb{R}^M , while $\mathbf{0}_M$ and $\mathbf{1}_M$ are the vectors of dimension M with all zeros and ones, respectively. Symbol $\mathbb{E}\{\cdot\}$ denotes expectation, $\mathbb{P}\{\cdot\}$ probability, $\text{Tr}(\cdot)$ trace, $\lambda_{\max}(\cdot)$ largest eigenvalue, and \star convolution. Notation $\lceil \rho \rceil$ (alternatively $\lfloor \rho \rfloor$) represents the smallest (largest) integer z satisfying $z \geq \rho$ ($z \leq \rho$).

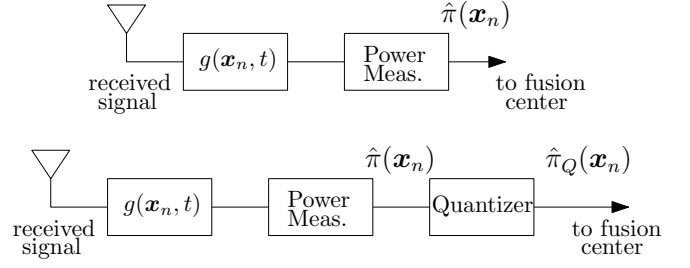


Fig. 1: Sensor architectures without (top) and with (bottom) quantization.

II. SYSTEM MODEL AND PROBLEM STATEMENT

Consider $M - 1$ sources located over a geographical region \mathcal{R} , where $\mathcal{R} \subset \mathbb{R}^d$ (d is typically 1, 2 or 3). Let $\phi_m(f)$ denote the transmit-PSD of the m th source. Without loss of generality, $\phi_m(f)$ is normalized to $\int_{-\infty}^{\infty} \phi_m(f) df = 1$, absorbing any scaling factor (which represents power) into the propagation channel. Assume that the channel from source m to location $\mathbf{x} \in \mathcal{R}$ is frequency flat (see Remark 1), and represent its gain by $l_m(\mathbf{x})$. If the $M - 1$ signals are uncorrelated, the PSD at location \mathbf{x} is given by the superposition

$$\Gamma(\mathbf{x}, f) = \sum_{m=1}^M l_m(\mathbf{x}) \phi_m(f) \quad (1)$$

where $\phi_M(f)$ is the normalized noise PSD, and $l_M(\mathbf{x})$ denotes the noise power.

Often in practice, transmit-sources adhere to publicly available standards and regulations, which prescribe spectral masks, bandwidths, carrier frequencies, roll-off factors, number of pilots, and positions of the pilots. For this reason, the normalized PSDs $\{\phi_m(f)\}_{m=1}^{M-1}$ are typically known [30], [37], at least approximately. If unknown, the methods here carry over after replacing source PSDs with general frequency-domain basis expansion models [6], [8].

The goal is to estimate the PSD map $\Gamma(\mathbf{x}, f)$ relying on the measurements of N sensors with locations $\{\mathbf{x}_n\}_{n=1}^N \subset \mathbb{R}^d$. For known $\{\phi_m(f)\}_{m=1}^{M-1}$, this task is tantamount to estimating $\{l_m(\mathbf{x})\}_{m=1}^M$ at every spatial coordinate \mathbf{x} . To minimize hardware cost and power consumption, this paper proposes the sensor architecture schematically described in Fig. 1. With $G(\mathbf{x}_n, f)$ denoting the frequency response of the time-invariant receive-filter $g(\mathbf{x}_n, f)$ of the n th sensor, the ensemble power at its output is $\pi(\mathbf{x}_n) = \int_{-\infty}^{\infty} |G(\mathbf{x}_n, f)|^2 \Gamma(\mathbf{x}_n, f) df$, which after substituting (1) can be re-written as

$$\pi(\mathbf{x}_n) = \sum_{m=1}^M l_m(\mathbf{x}_n) \Phi_m(\mathbf{x}_n) = \boldsymbol{\phi}^T(\mathbf{x}_n) \mathbf{l}(\mathbf{x}_n) \quad (2)$$

where $\Phi_m(\mathbf{x}_n) := \int_{-\infty}^{\infty} |G(\mathbf{x}_n, f)|^2 \phi_m(f) df$, while $\boldsymbol{\phi}(\mathbf{x}_n) := [\Phi_1(\mathbf{x}_n), \dots, \Phi_M(\mathbf{x}_n)]^T$, and $\mathbf{l}(\mathbf{x}_n) := [l_1(\mathbf{x}_n), \dots, l_M(\mathbf{x}_n)]^T$. The sensor estimates $\pi(\mathbf{x}_n)$ using e.g. a sample average $\hat{\pi}(\mathbf{x}_n)$ and sends the result to the fusion center.

To further reduce communication bandwidth, $\hat{\pi}(\mathbf{x}_n)$ can be uniformly quantized (see also Remark 5) as

$$\hat{\pi}_Q(\mathbf{x}_n) := Q(\hat{\pi}(\mathbf{x}_n)) := \lfloor \hat{\pi}(\mathbf{x}_n) / (2\epsilon) \rfloor, \quad n = 1, \dots, N \quad (3)$$

where 2ϵ is the quantization step. Depending on how accurate $\hat{\pi}(\mathbf{x}_n)$ is, either $Q(\pi(\mathbf{x}_n)) = Q(\hat{\pi}(\mathbf{x}_n))$ or $Q(\pi(\mathbf{x}_n)) \neq Q(\hat{\pi}(\mathbf{x}_n))$. The latter event is termed *measurement error* and occurs since $\hat{\pi}(\mathbf{x}_n)$ is obtained by averaging over a finite number of samples.

Having communicated the low-overhead measurements $\{\hat{\pi}(\mathbf{x}_n)\}_{n=1}^N$ or $\{\hat{\pi}_Q(\mathbf{x}_n)\}_{n=1}^N$ to a fusion center, which also knows $\{\phi_m(f)\}_{m=1}^M$ and $\{\mathbf{x}_n\}_{n=1}^N$, the *problem* is to estimate $\{l_m(\mathbf{x})\}_{m=1}^M$ (and thus $\Gamma(\mathbf{x}, f)$ in (1)) at every \mathbf{x} . The latter can be viewed individually as M functions of the spatial coordinate \mathbf{x} , or, altogether as a vector field $\mathbf{l} : \mathbb{R}^d \rightarrow \mathbb{R}^M$, where $\mathbf{l}(\mathbf{x}) := [l_1(\mathbf{x}), \dots, l_M(\mathbf{x})]^T$. Thus, estimating the PSD map in (1) is fact a function estimation problem.

Remark 1 (Frequency-selective channels). *If the channels are not frequency-flat, then each term in the sum of (1) can be decomposed into multiple components of lower bandwidth in such a way that each one undergoes an approximately frequency-flat channel. Choosing them to have disjoint frequency support ensures that they are uncorrelated and thus (1) remains valid.*

Remark 2. *The receive-filters can have pseudo-random impulse response and $\hat{\pi}(\mathbf{x}_n)$ can be obtained averaging squared samples of the filter output via digital processing [25]. Selecting distinct seeds for the random number generators of different sensors yields linearly independent $\{\phi(\mathbf{x}_n)\}_{n=1}^N$ with high probability, which ensures identifiability of $\{l_m(\mathbf{x}_n)\}_{m=1}^M$ (cf. (2)).*

Remark 3. *If Nyquist-rate sampling is too demanding for low-cost sensors (possible when estimating wideband maps), one can replace the filter in Fig. 1 with an analog-to-information-converter (A2IC) [30], [36]. To see that (2) still holds, let $\mathbf{G}(\mathbf{x}_n)$ represent the compression matrix of the n th sensor, which multiplies raw measurement blocks to yield compressed data blocks [30]. The ensemble power of the latter is proportional to $\pi(\mathbf{x}_n) := \text{Tr}(\mathbf{G}(\mathbf{x}_n)\boldsymbol{\Sigma}(\mathbf{x}_n)\mathbf{G}^T(\mathbf{x}_n))$, where $\boldsymbol{\Sigma}(\mathbf{x}_n) = \sum_{m=1}^M l_m(\mathbf{x}_n)\boldsymbol{\Sigma}_m$ denotes the covariance matrix of the uncompressed data blocks, and $\boldsymbol{\Sigma}_m$ the covariance matrix of the transmitted blocks from the m th source. Combining both equalities yields (2) upon defining $\Phi_m(\mathbf{x}_n) := \text{Tr}(\mathbf{G}(\mathbf{x}_n)\boldsymbol{\Sigma}_m\mathbf{G}^T(\mathbf{x}_n))$.*

III. LEARNING PSD MAPS

This section develops various PSD map estimators offering different bandwidth-performance trade-offs. The simplest one is developed in Sec. III-A by adopting a nonparametric regression approach to recover $\mathbf{l}(\mathbf{x}) := [l_1(\mathbf{x}) \dots l_M(\mathbf{x})]^T$ from unquantized measurements. To reduce bandwidth requirements, this approach is extended in Sec. III-B to accommodate quantized data. Since strong quantization deteriorates the quality of map estimates, a more sophisticated technique that counteracts this effect by leveraging propagation prior information is developed in Sec. III-C. For simplicity, these methods are presented for the scenario where a single measurement per sensor is available. Their general versions that utilize multiple measurements per sensor are outlined in Sec. III-D.

A. Estimation via nonparametric multivariate regression

Function estimation is intrinsically an ill-conditioned problem since any finite set of samples generally admits infinitely many interpolants. A contemporary framework ensuring a unique estimate is kernel-based regression, which seeks the desired function by minimizing the sum of two terms. The first is a fitting loss that penalizes estimates deviating from the observations. The second is a regularizer that promotes smoothness to limit overfitting.

Kernel-based regression seeks estimates in a wide class of functions termed *reproducing kernel Hilbert space* (RKHS), which in the present M -variate setting is given by $\mathcal{H} := \{\mathbf{l}(\mathbf{x}) = \sum_{n=1}^{\infty} \mathbf{K}(\mathbf{x}, \tilde{\mathbf{x}}_n)\tilde{\mathbf{c}}_n : \tilde{\mathbf{x}}_n \in \mathbb{R}^d, \tilde{\mathbf{c}}_n \in \mathbb{R}^M\}$ [11], [26]. In this expression, $\{\tilde{\mathbf{c}}_n\}_{n=1}^{\infty}$ are $M \times 1$ expansion coefficient vectors. The so-called reproducing kernel map $\mathbf{K}(\mathbf{x}, \mathbf{x}') : \mathbb{R}^d \times \mathbb{R}^d \rightarrow \mathbb{R}^{M \times M}$ satisfies three properties: (p1) $\mathbf{K}(\mathbf{x}, \mathbf{x}') = \mathbf{K}(\mathbf{x}', \mathbf{x})$ and $\mathbf{K}(\mathbf{x}, \mathbf{x})$ is positive semi-definite for all \mathbf{x}, \mathbf{x}' ; (p2) with $\langle \cdot, \cdot \rangle_{\mathcal{H}}$ denoting the inner product on \mathcal{H} , the reproducing property $\langle \mathbf{K}(\mathbf{x}, \cdot)\tilde{\mathbf{c}}, \mathbf{K}(\mathbf{x}', \cdot)\tilde{\mathbf{c}}' \rangle_{\mathcal{H}} = \tilde{\mathbf{c}}^T \mathbf{K}(\mathbf{x}, \mathbf{x}')\tilde{\mathbf{c}}'$ holds $\forall \tilde{\mathbf{c}}, \tilde{\mathbf{c}}'$, where the symbol \cdot can be thought of as a dummy variable; and, (p3) for any $\{\tilde{\mathbf{x}}_1, \dots, \tilde{\mathbf{x}}_N\}$, the square matrix having $\mathbf{K}(\tilde{\mathbf{x}}_n, \tilde{\mathbf{x}}_{n'})$ as its (n, n') block is positive semi-definite. Thanks to (p2), the RKHS norm is expressible as $\|\mathbf{l}\|_{\mathcal{H}}^2 := \langle \mathbf{l}, \mathbf{l} \rangle = \sum_{n=1}^{\infty} \sum_{n'=1}^{\infty} \tilde{\mathbf{c}}_n^T \mathbf{K}(\tilde{\mathbf{x}}_n, \tilde{\mathbf{x}}_{n'})\tilde{\mathbf{c}}_{n'}$. Remark 4 guides the selection of a reproducing kernel satisfying these properties.

With $\mathcal{L}(e_n)$ denoting a loss function of the error $e_n := \hat{\pi}(\mathbf{x}_n) - \phi^T(\mathbf{x}_n)\mathbf{l}(\mathbf{x}_n)$, the nonparametric kernel-based regression estimate is [9]

$$\hat{\mathbf{l}} \in \arg \min_{\mathbf{l} \in \mathcal{H}} \frac{1}{N} \sum_{n=1}^N \mathcal{L}(\hat{\pi}(\mathbf{x}_n) - \phi^T(\mathbf{x}_n)\mathbf{l}(\mathbf{x}_n)) + \lambda \|\mathbf{l}\|_{\mathcal{H}}^2 \quad (4)$$

where the user-selected scalar λ controls the tradeoff between the empirical fit of the given data, and the smoothness of the wanted function captured by its norm (as in parametric ridge regression). Since \mathcal{H} is infinite-dimensional, solving (4) directly is not generally possible with a finite number of operations. Fortunately, the *representer theorem* (see e.g., [2], [31]) asserts that $\hat{\mathbf{l}}$ in (4) is of the form

$$\sum_{n=1}^N \mathbf{K}(\mathbf{x}, \mathbf{x}_n)\mathbf{c}_n := \mathbf{K}(\mathbf{x})\mathbf{c} \quad (5)$$

for some $\{\mathbf{c}_n\}_{n=1}^N$, where $\mathbf{K}(\mathbf{x}) := [\mathbf{K}(\mathbf{x}, \mathbf{x}_1) \dots \mathbf{K}(\mathbf{x}, \mathbf{x}_N)]$ has size $M \times MN$, and $\mathbf{c} := [\mathbf{c}_1^T \dots \mathbf{c}_N^T]^T$ is $MN \times 1$. In words, the solution to (4) admits a kernel expansion around the sensor locations. From (5), it follows that finding $\hat{\mathbf{l}}$ amounts to finding \mathbf{c} . The latter can be obtained by solving the problem that results from substituting (5) into (4):

$$\hat{\mathbf{c}} \in \arg \min_{\mathbf{c}} \sum_{n=1}^N \mathcal{L}(\hat{\pi}(\mathbf{x}_n) - \phi^T(\mathbf{x}_n)\mathbf{K}(\mathbf{x}_n)\mathbf{c}) + \lambda N \mathbf{c}^T \mathbf{K} \mathbf{c}. \quad (6)$$

In (6), the $MN \times MN$ matrix \mathbf{K} is formed to have $\mathbf{K}(\mathbf{x}_n, \mathbf{x}_{n'})$ as its (n, n') th block. The minimizer of (4) can be then recovered as $\hat{\mathbf{l}}(\mathbf{x}) = \mathbf{K}(\mathbf{x})\hat{\mathbf{c}}$.

The popular *ridge regression* estimator is found when \mathcal{L} is the squared loss $\mathcal{L}_2(e_n) := e_n^2$, for which (6) becomes

$$\hat{\mathbf{c}} \in \arg \min_{\mathbf{c} \in \mathbb{R}^{MN}} \|\hat{\boldsymbol{\pi}} - \Phi_0^T \mathbf{K} \mathbf{c}\|_2^2 + \lambda N \mathbf{c}^T \mathbf{K} \mathbf{c}$$

where $\hat{\boldsymbol{\pi}} := [\hat{\pi}(\mathbf{x}_1) \dots \hat{\pi}(\mathbf{x}_N)]^T$ and $\Phi_0 := \mathbf{I}_N \odot \Phi$, with $\Phi := [\phi(\mathbf{x}_1) \dots \phi(\mathbf{x}_N)]$. The closed form solution is

$$\hat{\mathbf{c}} = (\Phi_0 \Phi_0^T \mathbf{K} + \lambda N \mathbf{I}_{MN})^{-1} \Phi_0 \hat{\boldsymbol{\pi}}. \quad (7)$$

In addition to its simplicity of implementation, the estimate $\hat{\mathbf{l}}(\mathbf{x}) = \mathbf{K}(\mathbf{x})\hat{\mathbf{c}}$, with $\hat{\mathbf{c}}$ as in (7), offers a twofold advantage over competing alternatives. First, existing methods relying on *power measurements* can only construct *power maps* [1], [18], [19], [22], [23], whereas the proposed method is capable of obtaining *PSD maps* from the same measurements. On the other hand, existing methods for estimating *PSD maps* require *PSD measurements*, that is, every sensor must obtain and transmit periodograms to the fusion center. This entails higher communication bandwidths, longer sensing times, and more costly sensors than required for the proposed scheme [6], [8], [13].

Remark 4. *Similar to the scalar case, the choice of the kernel considerably affects the estimation performance, especially when the number of observations is small. Thus, it is important to choose a kernel well-suited to the variability of the true \mathbf{l} across space. To do so, one may rely on cross validation, historical data [31, Sec. 2.3], or multi-kernel approaches [7]. Although specifying multivariate kernels is more challenging than specifying their scalar counterparts ($M = 1$) [26], it is possible to start with valid scalar kernels $\{k_m(\mathbf{x}, \mathbf{x}')\}_{m=1}^M$ and construct e.g. a diagonal kernel as $\mathbf{K}(\mathbf{x}, \mathbf{x}') = \text{diag}(k_1(\mathbf{x}, \mathbf{x}'), \dots, k_M(\mathbf{x}, \mathbf{x}'))$. It can be seen that the latter is a valid kernel for the M -variate case. A multivariate generalization of the popular Gaussian kernel can be found in this way by setting $k_m(\mathbf{x}, \mathbf{x}') = \exp(-\|\mathbf{x} - \mathbf{x}'\|^2 / \sigma_m^2)$.*

B. Nonparametric multivariate regression using quantized data

The scheme in Sec. III-B offers a drastic bandwidth reduction relative to competing PSD map estimators since only scalar-valued power measurements need to be communicated to the fusion center. To effect further bandwidth reductions, the power measurements $\{\hat{\pi}(\mathbf{x}_n)\}_{n=1}^N$ can be quantized (see bottom of Fig. 1) to $\lceil \log_2 R \rceil$ bits, where R denotes the number of quantization levels. The quantized measurements $\{\hat{\pi}_Q(\mathbf{x}_n)\}_{n=1}^N$ essentially convey *interval information*, in the sense that $\hat{\pi}(\mathbf{x}_n)$ is contained in the interval $[y(\mathbf{x}_n) - \epsilon, y(\mathbf{x}_n) + \epsilon)$, where $y(\mathbf{x}_n) := [2\hat{\pi}_Q(\mathbf{x}_n) + 1]\epsilon$ denotes the centroid of the quantization interval indexed by $\hat{\pi}_Q(\mathbf{x}_n)$. To account for the uncertainty within such an interval, one can solve (4) with $y(\mathbf{x}_n)$ in place of $\hat{\pi}(\mathbf{x}_n)$ as

$$\hat{\mathbf{l}} \in \arg \min_{\mathbf{l} \in \mathcal{H}} \frac{1}{N} \sum_{n=1}^N \mathcal{L}(y(\mathbf{x}_n) - \phi^T(\mathbf{x}_n)\mathbf{l}(\mathbf{x}_n)) + \lambda \|\mathbf{l}\|_{\mathcal{H}}^2 \quad (8)$$

and with a fitting loss \mathcal{L} assigning no cost across all candidate functions \mathbf{l} that lead to values of $\pi(\mathbf{x}_n) = \phi^T(\mathbf{x}_n)\mathbf{l}(\mathbf{x}_n)$ falling $\pm\epsilon$ around $y(\mathbf{x}_n)$; that is, such \mathcal{L} only penalizes functions \mathbf{l} for which $e_n = y(\mathbf{x}_n) - \phi^T(\mathbf{x}_n)\mathbf{l}(\mathbf{x}_n)$ falls outside

$[-\epsilon, \epsilon)$. Examples of these ϵ -insensitive loss functions include $\mathcal{L}_{1\epsilon}(e_n) := \max(0, |e_n| - \epsilon)$ [31], [33], and the less known $\mathcal{L}_{2\epsilon}(e_n) := \max(0, e_n^2 - \epsilon)$, both of which effect sparsity in $\{e_n\}_{n=1}^N$. This property is particularly well-motivated when the number of measurement errors is small relative to N , that is, when $Q(\pi(\mathbf{x}_n)) = Q(\hat{\pi}(\mathbf{x}_n))$ for *most* values of n .

The $\mathcal{L}_{1\epsilon}$ and $\mathcal{L}_{2\epsilon}$ losses not only give rise to convex criteria, but also allow dual-domain solvers with worst-case complexity $\mathcal{O}(N^{3.5})$ that does not grow with M . To establish this, note that application of the representer theorem to (8) yields, as in Sec. III-A, an estimate $\hat{\mathbf{l}}(\mathbf{x}) = \mathbf{K}(\mathbf{x})\hat{\mathbf{c}}$ with

$$\hat{\mathbf{c}} \in \arg \min_{\mathbf{c}} \sum_{n=1}^N \mathcal{L}(y(\mathbf{x}_n) - \phi^T(\mathbf{x}_n)\mathbf{K}(\mathbf{x}_n)\mathbf{c}) + \lambda N \mathbf{c}^T \mathbf{K} \mathbf{c}. \quad (9)$$

Now focus on $\mathcal{L}_{1\epsilon}$ and note that $\mathcal{L}_{1\epsilon}(e_n) = \xi_n + \zeta_n$, where $\xi_n := \max(0, e_n - \epsilon)$ and $\zeta_n := \max(0, -e_n - \epsilon)$ respectively quantify positive deviations of e_n with respect to the right and left endpoints of $[-\epsilon, \epsilon)$. This implies that ξ_n satisfies $\xi_n \geq e_n - \epsilon$ and $\xi_n \geq 0$, whereas ζ_n satisfies $\zeta_n \geq -e_n - \epsilon$ and $\zeta_n \geq 0$; thus establishing the following result.

Proposition 1. *The optimization in (9) with \mathcal{L} the ϵ -insensitive loss function $\mathcal{L}_{1\epsilon}$ can be expressed as*

$$\begin{aligned} (\hat{\mathbf{c}}, \hat{\boldsymbol{\xi}}, \hat{\boldsymbol{\zeta}}) \in \arg \min_{\mathbf{c}, \boldsymbol{\xi}, \boldsymbol{\zeta}} \sum_{n=1}^N (\xi_n + \zeta_n) + \lambda N \mathbf{c}^T \mathbf{K} \mathbf{c} \quad (10) \\ \text{s.t. } \xi_n \geq y(\mathbf{x}_n) - \phi^T(\mathbf{x}_n)\mathbf{K}(\mathbf{x}_n)\mathbf{c} - \epsilon, \quad \xi_n \geq 0, \\ \zeta_n \geq -y(\mathbf{x}_n) + \phi^T(\mathbf{x}_n)\mathbf{K}(\mathbf{x}_n)\mathbf{c} - \epsilon, \quad \zeta_n \geq 0, \\ n = 1, \dots, N \end{aligned}$$

where $\boldsymbol{\xi} := [\xi_1, \dots, \xi_N]^T$ and $\boldsymbol{\zeta} := [\zeta_1, \dots, \zeta_N]^T$.

Problem (10) is a quadratic program with slack variables $\{\xi_n, \zeta_n\}_{n=1}^N$. To the best of our knowledge, (10) constitutes the first application of an ϵ -insensitive loss to estimating functions from quantized samples. As expected from the choice of loss function and regularizer, problem (10) is an SVM-type problem. Specifically, letting $\tilde{\mathbf{c}} := \mathbf{K}^{1/2}\mathbf{c}$ renders the objective in (10) resemble that of a canonical (linear) SVM devoid of the offset term. However, it differs from SVM since the dimension of the primal vector $\tilde{\mathbf{c}}$ grows with the data and the constraints involve the kernel function. If on the other hand one is tempted to view the objective as that of kernel-based support vector regression (SVR), there is again discrepancy because of the vectors $\phi^T(\mathbf{x}_n)$ that pre-multiply $\mathbf{K}(\mathbf{x}_n)$ in the constraints. Nonetheless, this link with SVM-type formulations endows the proposed estimate with the universality of SVMs, which enjoy well-documented generalization performance [11], [26], [34].

While recognizing the merits that the proposed estimator inherits from SVM solvers, it is prudent to highlight one extra notable difference between (10) and SVM that pertains to ϵ . In the present setting, this parameter is fixed by the quantizer to half the quantization interval length, whereas in SVM it must be delicately tuned to control generalization performance.

The proposed estimator is termed *nonparametric* since the number of unknowns depends on the number of observations N . Although the number of unknowns also grows with M ,

it is shown next that this is not the case in the dual formulation. To see this, let $\mathbf{K}_0 := \Phi_0^T \mathbf{K} \Phi_0$ as well as $\mathbf{y} := [y(\mathbf{x}_1) \dots y(\mathbf{x}_N)]^T$. With α and β representing the Lagrange multipliers associated with the $\{\xi_n\}$ and the $\{\zeta_n\}$ constraints, the dual of (10) is

$$(\hat{\alpha}, \hat{\beta}) \in \arg \min_{\alpha, \beta \in \mathbb{R}^N} \frac{1}{4N\lambda} (\alpha - \beta)^T \mathbf{K}_0 (\alpha - \beta) - (\mathbf{y} - \epsilon \mathbf{1}_N)^T \alpha + (\mathbf{y} + \epsilon \mathbf{1}_N)^T \beta \quad (11)$$

$$\text{s. to} \quad \mathbf{0}_N \leq \alpha \leq \mathbf{1}_N, \mathbf{0}_N \leq \beta \leq \mathbf{1}_N.$$

From the Karush-Kuhn-Tucker (KKT) conditions, the primal variables can be recovered from the dual ones using

$$\hat{\mathbf{c}} = \frac{1}{2\lambda N} \Phi_0 (\hat{\alpha} - \hat{\beta}) \quad (12a)$$

$$\hat{\xi} = \max(\mathbf{0}_N, \mathbf{y} - \Phi_0^T \mathbf{K} \hat{\mathbf{c}} - \epsilon \mathbf{1}_N) \quad (12b)$$

$$\hat{\zeta} = \max(\mathbf{0}_N, -\mathbf{y} + \Phi_0^T \mathbf{K} \hat{\mathbf{c}} - \epsilon \mathbf{1}_N). \quad (12c)$$

Note that the primal (10) entails $(M+2)N$ variables whereas the dual (11) has $2N$. The dual in (11) can be solved using sequential minimal optimization algorithms [27], which here can afford simplified implementation along the lines of e.g., [20] because there is no bias term present. However, for moderate problem sizes ($< 5,000$), interior point solvers are more reliable [31, Ch. 10] while having *worst-case* complexity $\mathcal{O}(N^{3.5})$. As a desirable byproduct, interior point methods directly provide the Lagrange multipliers, which are useful for recovering the primal variables (cf. (22)).

C. Semiparametric multivariate regression using quantized data

Nonparametric estimators such as those in Sec. III-A and III-B are universal in the sense that they can approximate any continuous function l with arbitrary accuracy, provided that the number of measurements is large enough [11]. However, since the number of measurements is limited, incorporating available prior information is crucial to obtain accurate estimates. Furthermore, such prior information help counteract the negative impact of quantization in the quality of the PSD map estimate. On the other hand, *parametric* approaches readily accommodate various forms of prior information but lack the flexibility of nonparametric techniques. Semiparametric alternatives offer a ‘‘sweet spot’’ since they combine the merits of both approaches [31].

This section presents semiparametric estimators capable of capturing prior information about the propagation environment. Specifically, an estimate of the form $l(\mathbf{x}) = l'(\mathbf{x}) + \check{l}(\mathbf{x})$ is pursued, where (cf. Secs. III-A and III-B) the nonparametric component $l'(\mathbf{x})$ belongs to an RKHS \mathcal{H}' with kernel matrix \mathbf{K}' ; whereas the parametric component is given by

$$\check{l}(\mathbf{x}) = \sum_{\nu=1}^{N_B} \mathbf{B}_\nu(\mathbf{x}) \theta_\nu := \mathbf{B}(\mathbf{x}) \boldsymbol{\theta} \quad (13)$$

with $\mathbf{B}(\mathbf{x}) := [\mathbf{B}_1(\mathbf{x}) \dots \mathbf{B}_{N_B}(\mathbf{x})]$ collecting N_B known $M \times M$ basis matrix functions $\{\mathbf{B}_\nu(\mathbf{x})\}_{\nu=1}^{N_B}$ and $\boldsymbol{\theta} := [\theta_1^T \dots \theta_{N_B}^T]^T$.

If the source locations $\{\chi_m\}_{m=1}^M$ are approximately known, the propagation loss functions can be described by matrix basis functions of the form $\mathbf{B}_m(\mathbf{x}) = f_m(\|\mathbf{x} - \chi_m\|) \mathbf{e}_{M,m} \mathbf{e}_{M,m}^T$,

where $f_m(\|\mathbf{x} - \chi_m\|)$ models the attenuation at an arbitrary point \mathbf{x} as a function of the distance from a source located at χ_m . In this case, the vector θ_m to be estimated captures the power transmitted by source m .

One possible two-step approach to estimating l is to first fit the data with \check{l} in (13), and then fit the residuals with l' as detailed in the previous Sec. III-B. Since this so-termed *back-fitting* approach is known to yield sub-optimal estimates [31], this paper pursues a joint fit, which is novel in multivariate kernel regression. To this end, define \mathcal{H} as the space of functions l (not necessarily an RKHS) that can be written as $l = l' + \check{l}$, with $l' \in \mathcal{H}'$ and \check{l} as in (13). One can thereby seek semiparametric estimates of the form

$$\hat{l} \in \arg \min_{l \in \mathcal{H}} \frac{1}{N} \sum_{n=1}^N \mathcal{L}(y(\mathbf{x}_n) - \phi^T(\mathbf{x}_n) l(\mathbf{x}_n)) + \lambda \|l'\|_{\mathcal{H}'}^2 \quad (14)$$

where the regularizer involves only the nonparametric component through the norm $\|\cdot\|_{\mathcal{H}'}$ in \mathcal{H}' . Using [2, Th. 3.1], one can readily generalize the representer theorem in [31, Th. 4.3] to the present multivariate semiparametric case. This yields $\hat{l}(\mathbf{x}) = \mathbf{K}'(\mathbf{x}) \hat{\mathbf{c}}' + \mathbf{B}(\mathbf{x}) \hat{\boldsymbol{\theta}}$, where

$$(\hat{\mathbf{c}}', \hat{\boldsymbol{\theta}}) \in \arg \min_{\mathbf{c}', \boldsymbol{\theta}} \sum_{n=1}^N \mathcal{L}(y(\mathbf{x}_n) - \phi^T(\mathbf{x}_n) [\mathbf{K}'(\mathbf{x}_n) \mathbf{c}' + \mathbf{B}(\mathbf{x}_n) \boldsymbol{\theta}]) + \lambda N \mathbf{c}'^T \mathbf{K}' \mathbf{c}' \quad (15)$$

Comparing (9) with (15), and replacing $\mathbf{K}(\mathbf{x}_n) \mathbf{c}$ with $\mathbf{K}'(\mathbf{x}_n) \mathbf{c}' + \mathbf{B}(\mathbf{x}_n) \boldsymbol{\theta}$ yields the next result (cf. Proposition 1).

Proposition 2. *The optimization in (15) with \mathcal{L} the ϵ -insensitive loss function $\mathcal{L}_{1\epsilon}$ can be expressed as*

$$(\hat{\mathbf{c}}', \hat{\boldsymbol{\theta}}, \hat{\xi}, \hat{\zeta}) \in \arg \min_{\mathbf{c}', \boldsymbol{\theta}, \xi, \zeta} \sum_{n=1}^N (\xi_n + \zeta_n) + \lambda N \mathbf{c}'^T \mathbf{K}' \mathbf{c}'$$

s.to $\xi_n \geq y(\mathbf{x}_n) - \phi^T(\mathbf{x}_n) [\mathbf{K}'(\mathbf{x}_n) \mathbf{c}' + \mathbf{B}(\mathbf{x}_n) \boldsymbol{\theta}] - \epsilon$, $\xi_n \geq 0$
 $\zeta_n \geq -y(\mathbf{x}_n) + \phi^T(\mathbf{x}_n) [\mathbf{K}'(\mathbf{x}_n) \mathbf{c}' + \mathbf{B}(\mathbf{x}_n) \boldsymbol{\theta}] - \epsilon$, $\zeta_n \geq 0$
 $n = 1, \dots, N.$ (16)

The primal problem in (16) entails vectors of size MN , which motivates solving its dual version. Upon defining $\mathbf{B} := \sum_{n=1}^N \sum_{\nu=1}^{N_B} (\mathbf{e}_{N,n} \mathbf{e}_{N_B,\nu}^T) \otimes \mathbf{B}_\nu(\mathbf{x}_n)$, and recalling that α and β represent the Lagrange multipliers associated with the $\{\xi_n\}$ and $\{\zeta_n\}$ constraints, the dual of (16) is given by

$$(\hat{\alpha}, \hat{\beta}) \in \arg \min_{\alpha, \beta} \frac{1}{4N\lambda} (\alpha - \beta)^T \mathbf{K}'_0 (\alpha - \beta) - (\mathbf{y} - \epsilon \mathbf{1}_N)^T \alpha + (\mathbf{y} + \epsilon \mathbf{1}_N)^T \beta \quad (17)$$

$$\text{s. to} \quad \mathbf{0}_N \leq \alpha \leq \mathbf{1}_N, \mathbf{0}_N \leq \beta \leq \mathbf{1}_N$$

$$\mathbf{B}^T \Phi_0 (\alpha - \beta) = \mathbf{0}$$

where $\mathbf{K}'_0 := \Phi_0^T \mathbf{K}' \Phi_0$. Except for the last constraint and the usage of \mathbf{K}'_0 , (17) is identical to (11). Similar to (12a), the primal vector of the nonparametric component can be readily obtained from the KKT conditions as

$$\hat{\mathbf{c}}' = \frac{1}{2\lambda N} \Phi_0 (\hat{\alpha} - \hat{\beta}). \quad (18)$$

Although θ can also be obtained from the KKT conditions, the resulting expressions turn out to be numerically unstable. A more stable alternative can be found if the Lagrange multipliers associated with the solution of (17) are known — the case, e.g., when an interior-point algorithm is employed. Noting that (16) is the dual of (17) reveals that the primal variables are actually the Lagrange multipliers of (17). In particular, $\hat{\theta}$ is obtained from the multipliers associated with the last constraint of (17).

So far, the kernels considered were required to be positive definite. The remainder of this section will deal with an expanded class comprising the so-termed conditionally positive definite (CPD) kernels. CPD kernels are natural for estimation problems that are invariant to translations in the data [31, p. 52]. In the present application, this brings about the intuitively appealing property of a shifted estimate $l(\mathbf{x} - \mathbf{s})$ when the data are $\{\mathbf{x}_n - \mathbf{s}\}_{n=1}^N$ (for criteria of the form (9), this occurs if the kernel is translation invariant: $\mathbf{K}(\mathbf{x}_n - \mathbf{s}, \mathbf{x}_{n'} - \mathbf{s}) = \mathbf{K}(\mathbf{x}_n, \mathbf{x}_{n'})$). Broadening the scope of the proposed semiparametric approach to accommodate CPD kernels also offers a generalization of thin-plate splines (TPS), which have well-documented merits in capturing shadowing of propagation channels [8], to operate on quantized data.

Consider the following definition, which generalizes that of scalar CPD kernels [31, Sec. 2.4] to the multivariate setup:

Definition 1. A kernel $\mathbf{K}(\mathbf{x}_1, \mathbf{x}_2) : \mathbb{R}^d \times \mathbb{R}^d \rightarrow \mathbb{R}^M$ is CPD with respect to $\{\mathbf{B}_\nu(\mathbf{x})\}_{\nu=1}^{N_B}$ if satisfies $\mathbf{c}^T \mathbf{K} \mathbf{c} \geq 0$ for every finite set $\{\mathbf{x}_n\}_{n=1}^N$ and for all \mathbf{c} such that $\mathbf{B}^T \mathbf{c} = \mathbf{0}$.

Clearly, any positive definite kernel is also CPD. To see how this class of kernels can be accommodated in the present framework, note that (18) together with the last constraint in (17) show that the solution to (16) satisfies $\mathbf{B}^T \hat{\mathbf{c}}' = \mathbf{0}$. Therefore, (16) can be equivalently solved by confining the vectors \mathbf{c}' to lie in the null space of \mathbf{B}^T ; that is,

$$\begin{aligned} (\hat{\mathbf{c}}', \hat{\theta}, \hat{\xi}, \hat{\zeta}) &= \arg \min_{\mathbf{c}', \theta, \xi, \zeta} \mathbf{1}_N^T (\xi + \zeta) + \lambda N \mathbf{c}'^T \mathbf{K}' \mathbf{c}' \\ \text{s.t. } \xi &\geq \mathbf{y} - \Phi_0^T (\mathbf{K}' \mathbf{c}' + \mathbf{B}\theta) - \epsilon \mathbf{1}_N, \quad \xi \geq \mathbf{0}_N \\ \zeta &\geq -\mathbf{y} + \Phi_0^T (\mathbf{K}' \mathbf{c}' + \mathbf{B}\theta) - \epsilon \mathbf{1}_N, \quad \zeta \geq \mathbf{0}_N \\ \mathbf{B}^T \mathbf{c}' &= \mathbf{0}. \end{aligned} \quad (19)$$

The new equality constraint ensures that (19) is convex in the feasible set if $\mathbf{K}'(\mathbf{x}, \mathbf{x}')$ is CPD with respect to $\{\mathbf{B}_\nu(\mathbf{x})\}_{\nu=1}^{N_B}$. However, (19) is susceptible to numerical issues because the block matrix \mathbf{K}' may not be positive semidefinite. One can circumvent this difficulty by adopting a change of variables $\mathbf{c}' := \mathbf{P}_B^\perp \tilde{\mathbf{c}}$, where $\mathbf{P}_B^\perp := \mathbf{I}_{MN} - \mathbf{B}(\mathbf{B}^T \mathbf{B})^{-1} \mathbf{B}^T \in \mathbb{R}^{MN \times MN}$ is the orthogonal projection operator onto the null space of \mathbf{B}^T . This can be used to rewrite (19) as

$$\begin{aligned} (\hat{\tilde{\mathbf{c}}}, \hat{\theta}, \hat{\xi}, \hat{\zeta}) &= \arg \min_{\tilde{\mathbf{c}}, \theta, \xi, \zeta} \mathbf{1}_N^T (\xi + \zeta) + \lambda N \tilde{\mathbf{c}}^T \mathbf{P}_B^\perp \mathbf{K}' \mathbf{P}_B^\perp \tilde{\mathbf{c}} \\ \text{s.t. } \xi &\geq \mathbf{y} - \Phi_0^T (\mathbf{K}' \mathbf{P}_B^\perp \tilde{\mathbf{c}} + \mathbf{B}\theta) - \epsilon \mathbf{1}_N, \quad \xi \geq \mathbf{0}_N \\ \zeta &\geq -\mathbf{y} + \Phi_0^T (\mathbf{K}' \mathbf{P}_B^\perp \tilde{\mathbf{c}} + \mathbf{B}\theta) - \epsilon \mathbf{1}_N, \quad \zeta \geq \mathbf{0}_N \end{aligned} \quad (20)$$

where now $\mathbf{P}_B^\perp \mathbf{K}' \mathbf{P}_B^\perp$ is guaranteed to be positive semidefinite.

A similar argument applies to the dual formulation in (17), where for α and β feasible, it holds that $(\alpha - \beta)^T \mathbf{K}'_0 (\alpha - \beta) \geq$

0 with $\mathbf{K}'(\mathbf{x}, \mathbf{x}')$ CPD. To avoid numerical issues, observe that any feasible α, β satisfy $\Phi_0(\alpha - \beta) = \mathbf{P}_B^\perp \Phi_0(\alpha - \beta)$, and thus (17) reduces to

$$\begin{aligned} (\hat{\alpha}, \hat{\beta}) &= \arg \min_{\alpha, \beta} \frac{1}{4N\lambda} (\alpha - \beta)^T \tilde{\mathbf{K}} (\alpha - \beta) \\ &\quad - (\mathbf{y} - \epsilon \mathbf{1}_N)^T \alpha + (\mathbf{y} + \epsilon \mathbf{1}_N)^T \beta \\ \text{s. to } &\mathbf{B}^T \Phi_0 (\alpha - \beta) = \mathbf{0} \\ &\mathbf{0}_N \leq \alpha \leq \mathbf{1}_N, \mathbf{0}_N \leq \beta \leq \mathbf{1}_N \end{aligned} \quad (21)$$

where \mathbf{K}'_0 has been replaced with the positive semidefinite matrix $\tilde{\mathbf{K}} := \Phi_0^T \mathbf{P}_B^\perp \mathbf{K}' \mathbf{P}_B^\perp \Phi_0$. With this reformulation, although the optimal $\hat{\mathbf{c}}'$ can still be recovered from (18), $\hat{\theta}$ cannot be obtained as the vector μ of Lagrange multipliers associated with the equality constraint in (21). This is due to the change of variables, which alters (21) from being the dual of (20). As derived in Appendix A, $\hat{\theta}$ can instead be recovered as

$$\hat{\theta} = \mu - (\mathbf{B}^T \mathbf{B})^{-1} \mathbf{B}^T \mathbf{K}' \hat{\mathbf{c}}'. \quad (22)$$

Broadening the scope to include CPD kernels leads also to multivariate generalizations of TPS – arguably the most popular semiparametric interpolator, which in the scalar case derives its name because it mimics the shape of a thin metal plate that minimizes the bending energy when anchored at the data points [10]. With $\mathbf{x} := [x_1, \dots, x_d]^T$, the multivariate version of TPS has a parametric basis containing $\mathbf{B}_1(\mathbf{x}) = \mathbf{I}_M$, $\mathbf{B}_2(\mathbf{x}) = x_1 \mathbf{I}_M, \dots, \mathbf{B}_{1+d}(\mathbf{x}) = x_d \mathbf{I}_M$, and diagonal matrix kernel

$$\mathbf{K}'(\mathbf{x}_1, \mathbf{x}_2) = r(\|\mathbf{x}_1 - \mathbf{x}_2\|_2^2) \mathbf{I}_M \quad (23)$$

where $r(z)$ denotes the radial basis function

$$r(z) := \begin{cases} z^{2s-d} \log(z) & \text{if } d \text{ is even} \\ z^{2s-d} & \text{otherwise} \end{cases} \quad (24)$$

for a positive integer s typically set to $s = 2$ [38, eq. (2.4.9)], [8]. The kernel in (23) can be shown to be CPD with respect to $\{\mathbf{B}_\nu(\mathbf{x})\}_{\nu=1}^{1+d}$ [38, p. 32]. The norm in the RKHS \mathcal{H}' induced by (23), which can be evaluated as in Sec. III-A, admits the equivalent form

$$\|\mathbf{l}'\|_{\mathcal{H}'}^2 = \sum_{m=1}^M \int_{\mathbb{R}^d} \|\nabla^2 l_m(\mathbf{z})\|_F^2 d\mathbf{z}$$

where $\|\cdot\|_F$ denotes Frobenius norm, and ∇^2 the Hessian. Therefore, the RKHS norm of \mathcal{H}' captures the conventional notion of smoothness embedded in the magnitude of the second-order derivatives. Among other reasons, TPS are popular because they do not require parameter tuning, unlike e.g., Gaussian kernels, which need adjustment of their variance parameter. The novelty here is the generalization of TPS to multivariate regression from quantized observations. Different from [8], which relies on un-quantized periodograms, the proposed scheme is based on quantized power measurements.

D. Multiple measurements per sensor

For simplicity, it was assumed so far that each sensor collects and reports a single measurement to the fusion center. However, $P > 1$ measurements can be taken per sensor by changing the filter impulse response between measurements, or, by appropriately modifying the compression matrix in their A2ICs (cf. Remark 3). A naive approach would be to regard the P measurements per sensor as measurements from P different sensors at the same location. However, this increases the problem size by a factor of P , and one has to deal with a rank deficient kernel matrix \mathbf{K} of dimension MNP , which renders the solutions of (6), (9) and (15) non-unique.

A more efficient means of accommodating P measurements per sensor in the un-quantized scenario is to reformulate (4) as

$$\hat{\mathbf{l}} \in \arg \min_{\mathbf{l} \in \mathcal{H}} \frac{1}{NP} \sum_{n=1}^N \sum_{p=1}^P \mathcal{L}(\hat{\pi}_p(\mathbf{x}_n) - \phi_p^T(\mathbf{x}_n)\mathbf{l}(\mathbf{x}_n)) + \lambda \|\mathbf{l}\|_{\mathcal{H}}^2 \quad (25)$$

where $\hat{\pi}_p(\mathbf{x}_n)$ and $\phi_p(\mathbf{x}_n)$ correspond to the p -th measurement reported by the sensor located at \mathbf{x}_n . Collect the observations in $\hat{\boldsymbol{\pi}} := [\hat{\pi}_1(\mathbf{x}_1), \hat{\pi}_2(\mathbf{x}_1), \dots, \hat{\pi}_P(\mathbf{x}_N)]^T$, let $\bar{\boldsymbol{\Phi}} := [\phi_1(\mathbf{x}_1), \phi_2(\mathbf{x}_1), \dots, \phi_P(\mathbf{x}_N)]$, and $\bar{\boldsymbol{\Phi}}_0 := (\mathbf{I}_N \otimes \mathbf{1}_P^T) \odot \bar{\boldsymbol{\Phi}} \in \mathbb{R}^{MN \times NP}$. As before, the representer theorem implies that the minimizer of (25) is given by $\hat{\mathbf{l}}(\mathbf{x}) = \sum_{n=1}^N \mathbf{K}(\mathbf{x}, \mathbf{x}_n) \hat{\mathbf{c}}_n := \mathbf{K}(\mathbf{x})\hat{\mathbf{c}}$. If \mathcal{L} is the square loss \mathcal{L}_2 (see Sec. III-A), then

$$\hat{\mathbf{c}} = (\bar{\boldsymbol{\Phi}}_0 \bar{\boldsymbol{\Phi}}_0^T \mathbf{K} + \lambda N \mathbf{I}_{MN})^{-1} \bar{\boldsymbol{\Phi}}_0 \hat{\boldsymbol{\pi}} \quad (26)$$

which generalizes (7) to $P \geq 1$. Note however that $\bar{\mathbf{c}}$ has dimension MN , rather than MNP , which is the dimension that would result if the naive approach were employed. Likewise, \mathbf{K} still has dimensionality $MN \times MN$.

If $\hat{\pi}_p(\mathbf{x}_n)$ is replaced with $y_p(\mathbf{x}_n)$ in (25), the resulting expression extends (8) to multiple measurements per sensor. If \mathcal{L} is the ϵ -insensitive cost $\mathcal{L}_{1\epsilon}$, such an expression is minimized for $\hat{\mathbf{l}}(\mathbf{x}) = \mathbf{K}(\mathbf{x})\hat{\mathbf{c}}$ with

$$\begin{aligned} (\hat{\mathbf{c}}, \hat{\boldsymbol{\xi}}, \hat{\boldsymbol{\zeta}}) \in \arg \min_{\mathbf{c}, \boldsymbol{\xi}, \boldsymbol{\zeta}} \mathbf{1}_{NP}^T (\bar{\boldsymbol{\xi}} + \bar{\boldsymbol{\zeta}}) + \lambda NP \bar{\mathbf{c}}^T \mathbf{K} \bar{\mathbf{c}} \\ \text{s. to } \bar{\boldsymbol{\xi}} \geq \bar{\mathbf{y}} - \bar{\boldsymbol{\Phi}}_0^T \mathbf{K} \bar{\mathbf{c}} - \epsilon \mathbf{1}_{NP}, \quad \bar{\boldsymbol{\xi}} \geq \mathbf{0}_{NP} \\ \bar{\boldsymbol{\zeta}} \geq -\bar{\mathbf{y}} + \bar{\boldsymbol{\Phi}}_0^T \mathbf{K} \bar{\mathbf{c}} - \epsilon \mathbf{1}_{NP}, \quad \bar{\boldsymbol{\zeta}} \geq \mathbf{0}_{NP} \end{aligned} \quad (27)$$

where $\bar{\mathbf{y}} := [y_1(\mathbf{x}_1), y_2(\mathbf{x}_1), \dots, y_P(\mathbf{x}_N)]^T$. Note that (27) reduces to (10) if $P = 1$. The dual formulation is the same as (11), except that $\boldsymbol{\alpha}$, $\boldsymbol{\beta}$, $\boldsymbol{\Phi}_0$, and N are replaced with $\bar{\boldsymbol{\alpha}}$, $\bar{\boldsymbol{\beta}}$, $\bar{\boldsymbol{\Phi}}_0$, and NP , respectively. The primal solution can be recovered as $\hat{\mathbf{c}} = (2\lambda NP)^{-1} \bar{\boldsymbol{\Phi}}_0 (\bar{\boldsymbol{\alpha}} - \bar{\boldsymbol{\beta}})$; cf. (12a).

The multi-measurement version of the semiparametric setup in (14) is

$$\hat{\mathbf{l}} \in \arg \min_{\mathbf{l} \in \mathcal{H}} \frac{1}{NP} \sum_{n=1}^N \sum_{p=1}^P \mathcal{L}(y_p(\mathbf{x}_n) - \phi_p^T(\mathbf{x}_n)\mathbf{l}(\mathbf{x}_n)) + \lambda \|\mathbf{l}\|_{\mathcal{H}}^2 \quad (28)$$

and the counterpart to (16) is obtained by replacing $\boldsymbol{\xi}$, $\boldsymbol{\zeta}$, \mathbf{y} , $\phi(\mathbf{x}_n)$ and N , with $\bar{\boldsymbol{\xi}}$, $\bar{\boldsymbol{\zeta}}$, $\bar{\mathbf{y}}$, $\phi_p(\mathbf{x}_n)$ and NP , respectively. Likewise, the dual formulation is obtained by substituting $\boldsymbol{\alpha}$, $\boldsymbol{\beta}$, $\boldsymbol{\Phi}_0$, N , and $\bar{\mathbf{K}}$ in (21) with $\bar{\boldsymbol{\alpha}}$, $\bar{\boldsymbol{\beta}}$, $\bar{\boldsymbol{\Phi}}_0$, NP , and

$$\bar{\mathbf{K}} := \bar{\boldsymbol{\Phi}}_0^T P_B^\perp \mathbf{K}' P_B \bar{\boldsymbol{\Phi}}_0 \quad (29)$$

respectively. The primal variables are recovered again as $\hat{\mathbf{c}} = (2\lambda NP)^{-1} \bar{\boldsymbol{\Phi}}_0 (\bar{\boldsymbol{\alpha}} - \bar{\boldsymbol{\beta}})$ and $\hat{\boldsymbol{\theta}} = \bar{\boldsymbol{\mu}} - (\mathbf{B}^T \mathbf{B})^{-1} \mathbf{B}^T \mathbf{K}' \hat{\mathbf{c}}$, where $\bar{\boldsymbol{\mu}}$ is the Lagrange multiplier vector associated with the equality constraints in the dual problem; cf. (22).

Remark 5 (Non-uniform quantization). *If $\hat{\pi}(\mathbf{x}_n)$ is not uniformly distributed, non-uniform quantization is well motivated over the uniform quantization adopted so far. With R quantization regions specified by the boundaries $0 = \tau_0 < \tau_1 < \dots < \tau_R$, the quantized measurements are $\pi_Q(\mathbf{x}_n) := Q(\hat{\pi}(\mathbf{x}_n)) = i$ if $\hat{\pi}(\mathbf{x}_n) \in [\tau_i, \tau_{i+1})$. The general formulations (25) and (28) can accommodate non-uniformly quantized observations by replacing the constant half interval ϵ in all relevant optimization problems with the variable one $\epsilon_n := (\tau_{\pi_Q(\mathbf{x}_n)+1} - \tau_{\pi_Q(\mathbf{x}_n)})/2$; and likewise modifying the centroid expression from $y(\mathbf{x}_n) := [2\pi_Q(\mathbf{x}_n) + 1]\epsilon$ to $y(\mathbf{x}_n) := (\tau_{\pi_Q(\mathbf{x}_n)+1} + \tau_{\pi_Q(\mathbf{x}_n)})/2$.*

Remark 6 (Enforcing nonnegativity). *Since all M entries of vector $\mathbf{l}(\mathbf{x})$ represent power, they are inherently nonnegative. One simple modification to enforce hard non-negativity of $\mathbf{l}(\mathbf{x})$ at all sensor locations is to introduce the constraint $\mathbf{K}(\mathbf{x}_n)\mathbf{c} \geq \mathbf{0}_M$ for $n = 1, \dots, N$ in (10). A soft alternative is to include M virtual measurements free of estimation error for every sensor location \mathbf{x}_n with $\phi_{P+m}(\mathbf{x}_n) = \mathbf{e}_{M,m}$ and $y_{P+m}(\mathbf{x}_n) := (\tau_0 + \tau_R)/2$ for $m = 1, \dots, M$, and quantization interval $2\epsilon := \tau_R - \tau_0$. Clearly, these virtual power measurements enforce constraints of the form $\mathbf{e}_{M,m}^T \mathbf{l}(\mathbf{x}_n) = l_m(\mathbf{x}_n) \in [\tau_0, \tau_R]$ for $n = 1, \dots, N$. These are indeed soft constraints since the empirical risk chosen assigns a finite penalty to any finite deviation from these intervals.*

Remark 7 (Computational complexity). *Utilizing un-quantized data, the estimate (26) requires $\mathcal{O}(M^3 N^3 + PM^2 N)$ operations. Regarding the nonparametric method based on quantized measurements, solving the dual of (27) using an interior point method takes $\mathcal{O}((NP)^{3.5})$ iterations. A similar level of complexity is incurred by its semiparametric counterpart. Albeit polynomial, this complexity may be prohibitive in real-time applications with limited computational capabilities if the number of measurements NP is large. For such scenarios, an online algorithm with linear complexity is proposed next, which is guaranteed to converge to the nonparametric estimate (9).*

IV. ONLINE ALGORITHM

The algorithms described so far operate in batch mode, thus requiring all observations to be gathered before training can commence. Moreover, their computational complexity increases faster than linear in NP , which may be prohibitive if the number of measurements is large relative to the available computational resources. These considerations motivate the development of online algorithms, which can both approximate the solution of the batch problem with complexity $\mathcal{O}(NP)$ and update $\hat{\mathbf{l}}(\mathbf{x})$ as new measurements arrive at the fusion center. As an additional motivation, online algorithms can also track slow variations over time in the field of interest.

Although online algorithms can be easily constructed by applying batch schemes over sliding windows [32], online strategies with instantaneous updates are preferred [14]. An elegant approach based on stochastic gradient descent (SGD) in the function space is developed in [24] for *scalar* kernel machines. Its *multivariate* counterpart, suitable for the present setting, is described in [4].

For a selected \mathcal{L} , consider the instantaneous regularized cost, defined for generic $\mathbf{l} \in \mathcal{H}$, \mathbf{x}_ν , $\phi(\mathbf{x}_\nu)$, and $y(\mathbf{x}_\nu)$ as

$$\mathcal{C}(\mathbf{l}, \phi(\mathbf{x}_\nu), \mathbf{x}_\nu, y(\mathbf{x}_\nu)) := \mathcal{L}(y(\mathbf{x}_\nu) - \phi^T(\mathbf{x}_\nu)\mathbf{l}(\mathbf{x}_\nu)) + \lambda \|\mathbf{l}\|_{\mathcal{H}}^2. \quad (30)$$

Note that (4) indeed minimizes the sample average of \mathcal{C} . Suppose that at time index $t = 1, 2, \dots$ the fusion center processes one measurement from sensor $n_t \in \{1, \dots, N\}$. If the fusion center uses multiple observations, say P , from the n_t 'th sensor, then $n_{t_1} = n_{t_2} = \dots = n_{t_P} = n_t$, where $\{t_1, \dots, t_P\}$ depends on the fusion center schedule.

Upon processing the t th measurement, the SGD update is

$$\mathbf{l}^{(t+1)} = \mathbf{l}^{(t)} - \mu_t \partial_l \mathcal{C}(\mathbf{l}^{(t)}, \phi(\mathbf{x}_{n_t}), \mathbf{x}_{n_t}, y(\mathbf{x}_{n_t})) \quad (31)$$

where $\mathbf{l}^{(t)}$ is the estimate at time t before $y(\mathbf{x}_{n_t})$ has been acquired; $\mu_t > 0$ is the learning rate; and ∂_l denotes subgradient with respect to \mathbf{l} . In general, μ_t can be replaced with a matrix \mathbf{M}_t to provide flexibility in tuning different components of \mathbf{l} . For \mathcal{C} as in (30), it can be shown using [4, eq. (2)] that

$$\begin{aligned} \partial_l \mathcal{C}(\mathbf{l}, \phi(\mathbf{x}_\nu), \mathbf{x}_\nu, y(\mathbf{x}_\nu))(\mathbf{x}) \\ = -\mathcal{L}'(y(\mathbf{x}_\nu) - \phi^T(\mathbf{x}_\nu)\mathbf{l}(\mathbf{x}_\nu))\mathbf{K}(\mathbf{x}, \mathbf{x}_\nu)\phi(\mathbf{x}_\nu) + 2\lambda\mathbf{l}(\mathbf{x}) \end{aligned} \quad (32)$$

and \mathcal{L}' is a subgradient of \mathcal{L} , which for $\mathcal{L}_{1\epsilon}(e_\nu) := \max(0, |e_\nu| - \epsilon)$ is e.g.:

$$\mathcal{L}'_{1\epsilon}(e_\nu) = \frac{\text{sgn}(e_\nu - \epsilon) + \text{sgn}(e_\nu + \epsilon)}{2}. \quad (33)$$

Substituting (32) into (31) yields

$$\begin{aligned} \mathbf{l}^{(t+1)}(\mathbf{x}) &= (1 - 2\mu_t\lambda)\mathbf{l}^{(t)}(\mathbf{x}) \\ &+ \mu_t\mathcal{L}'(y(\mathbf{x}_{n_t}) - \phi^T(\mathbf{x}_{n_t})\mathbf{l}^{(t)}(\mathbf{x}_{n_t}))\mathbf{K}(\mathbf{x}, \mathbf{x}_{n_t})\phi(\mathbf{x}_{n_t}). \end{aligned} \quad (34)$$

Upon setting $\mathbf{l}^{(1)} = \mathbf{0}$, it follows that

$$\mathbf{l}^{(t)}(\mathbf{x}) = \sum_{i=1}^{t-1} \mathbf{K}(\mathbf{x}, \mathbf{x}_{n_i})\mathbf{c}_i^{(t)} \quad (35)$$

for some $\mathbf{c}_i^{(t)}$, $i = 1, \dots, t-1$. Interestingly, although the representer theorem [26, Thm. 5] has not been invoked, the estimates $\mathbf{l}^{(t)}(\mathbf{x})$ here have the form of those in Sec. III.

If measurements come from sensors at different locations, the functions $\mathbf{K}(\mathbf{x}, \mathbf{x}_{n_i})$, $i = 1, \dots, t$, are linearly independent for properly selected kernels, and substituting (35) into (34) results in the following update rule

$$\mathbf{c}_i^{(t+1)} = (1 - 2\mu_t\lambda)\mathbf{c}_i^{(t)},$$

for $i = 1, \dots, t-1$, whereas for $i = t$,

$$\mathbf{c}_t^{(t+1)} = \mu_t\mathcal{L}'[y(\mathbf{x}_{n_t}) - \phi^T(\mathbf{x}_{n_t})\mathbf{l}^{(t)}(\mathbf{x}_{n_t})]\phi(\mathbf{x}_{n_t}).$$

These equations reveal that the number of coefficients maintained increases linearly in t . This is the so-called *curse of kernelization* [40]. However, note that if $\mu_t\lambda \in (0, 1)$, then the amplitudes of the entries in \mathbf{c}_i are shrunk by a factor of $|1 - 2\mu_t\lambda| < 1$. This justifies truncating (35) as

$$\mathbf{l}^{(t)}(\mathbf{x}) = \sum_{i=\max(1, t-I)}^{t-1} \mathbf{K}(\mathbf{x}, \mathbf{x}_i)\mathbf{c}_i^{(t)} \quad (36)$$

for some $I > 1$. On the other hand, if the fusion center processes multiple observations per sensor, $\{\mathbf{K}(\mathbf{x}, \mathbf{x}_{n_i})\}_{i=1}^t$ are no longer linearly independent. In such a case, up to N kernels $\{\mathbf{K}(\mathbf{x}, \mathbf{x}_n)\}_{n=1}^N$ are linearly independent, which yields

$$\mathbf{l}^{(t)}(\mathbf{x}) = \sum_{n=1}^N \mathbf{K}(\mathbf{x}, \mathbf{x}_n)\mathbf{c}_n^{(t)}. \quad (37)$$

After receiving the observation $(\mathbf{x}_{n_t}, y(\mathbf{x}_{n_t}), \phi(\mathbf{x}_{n_t}))$ at time t , (37) leads to the recursions

$$\mathbf{c}_n^{(t+1)} = (1 - 2\mu_t\lambda)\mathbf{c}_n^{(t)}$$

for $n \neq n_t$ and

$$\begin{aligned} \mathbf{c}_{n_t}^{(t+1)} &= (1 - 2\mu_t\lambda)\mathbf{c}_{n_t}^{(t)} \\ &+ \mu_t\mathcal{L}'[y(\mathbf{x}_{n_t}) - \phi^T(\mathbf{x}_{n_t})\mathbf{l}^{(t)}(\mathbf{x}_{n_t})]\phi(\mathbf{x}_{n_t}) \end{aligned}$$

for $n = n_t$. Convergence of these recursions is characterized by the next result, which adapts [4, Thm. 1] to the proposed setup.

Theorem 1. *If $\lambda_{\max}(\mathbf{K}(\mathbf{x}, \mathbf{x})) < \bar{\lambda}^2 < \infty$ for all \mathbf{x} , $\|\phi(\mathbf{x}_{n_t})\|_2 \leq \bar{\varphi}$ for all t , and $\mu_t := \mu t^{-1/2}$ with $\mu\lambda < 1$, then the iterates in (34) with $\mathcal{L} = \mathcal{L}_{1\epsilon}$ satisfy*

$$\frac{1}{T} \sum_{t=1}^T \mathcal{C}(\mathbf{l}^{(t)}, \phi(\mathbf{x}_{n_t}), \mathbf{x}_{n_t}, y(\mathbf{x}_{n_t})) \quad (38)$$

$$\leq \inf_{\mathbf{l} \in \mathcal{H}} \left[\frac{1}{T} \sum_{t=1}^T \mathcal{C}(\mathbf{l}, \phi(\mathbf{x}_{n_t}), \mathbf{x}_{n_t}, y(\mathbf{x}_{n_t})) \right] + \frac{c_1}{\sqrt{T}} + \frac{c_2}{T}$$

where $c_2 := \bar{\lambda}^2\bar{\varphi}^2/(8\lambda^2\mu)$ and $c_1 := 4(\bar{\lambda}^2\bar{\varphi}^2\mu + c_2)$.

Proof: See Appendix C. ■

In words, Theorem 1 establishes that the averaged instantaneous error from the online algorithm converges to the regularized empirical error of the batch solution.

V. NUMERICAL TESTS

Performance of the proposed algorithms was tested via numerical experiments. Following [17], a correlated shadow fading model was adopted, where, for $m = 1, \dots, M-1$,

$$10 \log l_m(\mathbf{x}) = 10 \log A_m - \gamma \log(\delta + \|\mathbf{x} - \boldsymbol{\chi}_m\|) + s_m(\mathbf{x}). \quad (39)$$

Here, δ is a small constant to ensure that the argument of the logarithm does not vanish, $\gamma = 3$ is the pathloss exponent, and the parameters A_m and $\boldsymbol{\chi}_m$ denote the transmit-power and the location of source m , respectively. The random shadowing component $s_m(\mathbf{x})$ is generated as a zero-mean Gaussian random

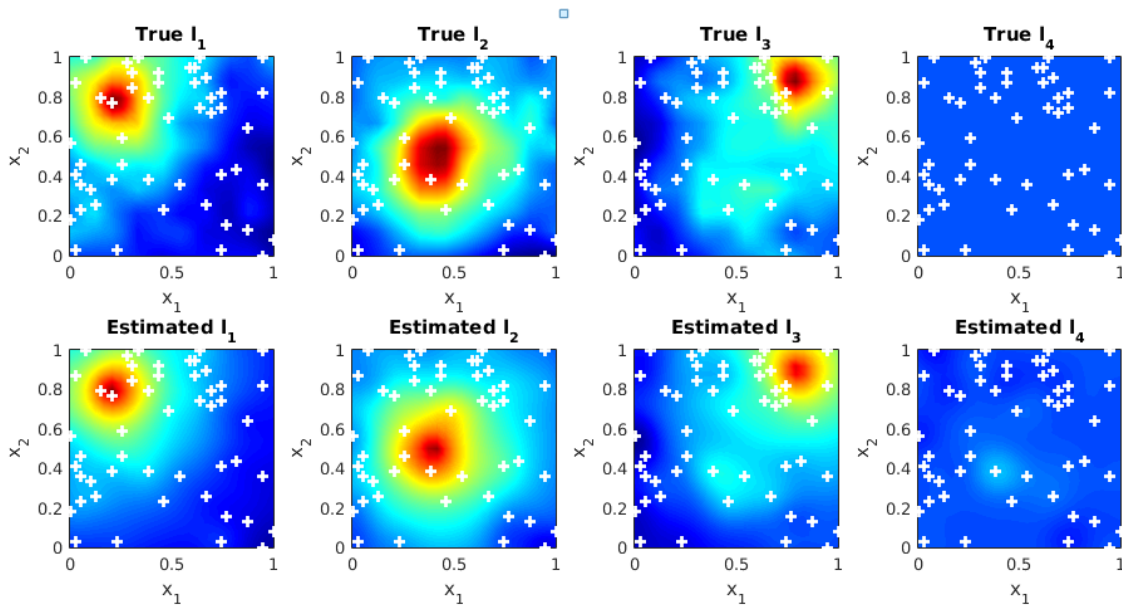


Fig. 2: True and estimated functions $l_m(\mathbf{x})$ when $N = 50$, $P = 8$, 5-bit quantization with CPQ, $\lambda = 10^{-9}$, and nonnegativity enforced. Each column corresponds to the power of a channel. White crosses denote sensor locations. The PSD at any location can be reconstructed by substituting the values of these functions into (1).

variable with $\mathbb{E}\{s_m(\mathbf{x})s_m(\mathbf{x}')\} = \sigma_s^2 \rho^{-\|\mathbf{x}-\mathbf{x}'\|}$, where $\sigma_s^2 = 2$ and $\rho = 0.8$. The noise power was set to $l_M(\mathbf{x}) = 0.75$.

The N sensors, deployed uniformly at random over the region of interest, report P quantized measurements $\{\hat{\pi}_{Q,p}(\mathbf{x}_n) = Q(|\pi_p(\mathbf{x}_n) + \eta_p(\mathbf{x}_n)|) = Q(|\phi_p^T(\mathbf{x}_n)\mathbf{l}(\mathbf{x}_n) + \eta_p(\mathbf{x}_n)|)\}_{p=1}^P$ to the fusion center, where $\eta_p(\mathbf{x}_n) \sim \mathcal{N}(0, \sigma_\eta^2)$ denotes noise due to finite sample estimation effects. The entries of $\phi_p(\mathbf{x}_n)$ were generated uniformly over the interval $[0, 1]$ for all \mathbf{x}_n and p .

Two quantization schemes were implemented. Under uniform quantization (UQ), the range of $\pi_p(\mathbf{x})$ was first determined using Monte Carlo runs and the quantization region boundaries $\tau_0 < \tau_1 < \dots < \tau_R$ were set such that $\tau_{i+1} - \tau_i = 2\epsilon \forall i$, where ϵ was such that the probability of clipping $\Pr\{\pi_p(\mathbf{x}) > \tau_R\}$ was approximately 10^{-3} and $R := 2^b$, with b the number of bits per measurement. Under constant probability quantization (CPQ), these boundaries were chosen such that $\Pr\{\tau_i \leq \pi_p(\mathbf{x}) < \tau_{i+1}\}$ was approximately constant for all i .

A PSD map in the region $[0, 1] \times [0, 1] \subset \mathbb{R}^2$ ($d = 2$) with $M - 1 = 3$ sources was constructed. The propagation parameters were $A_1 = 0.9$, $A_2 = 0.8$, $A_3 = 0.7$, $\mathbf{x}_1 = (0.2, 0.8)$, $\mathbf{x}_2 = (0.4, 0.5)$, and $\mathbf{x}_3 = (0.8, 0.9)$. A CPQ scheme was employed, nonnegativity was enforced using M virtual measurements per sensor, and the batch semiparametric estimate from (28) is computed. The nonparametric part adopts a diagonal Gaussian kernel matrix $\mathbf{K}(\mathbf{x}_n, \mathbf{x}_{n'})$ with $k_m(\mathbf{x}_n, \mathbf{x}_{n'}) = \exp(-\|\mathbf{x}_n - \mathbf{x}_{n'}\|^2 / \sigma_m^2)$ on its diagonal (cf. Remark 4), where $\sigma_m^2 = 0.12$ for $m = 1, 2, 3, 4$. The parametric part is spanned by a basis with $N_B = 1$ and $\mathbf{B}_1(\mathbf{x})$ a diagonal matrix whose (m, m) -th entry is given by $1/(\delta + \|\mathbf{x} - \chi_m\|^\gamma)$ if $m = 1, \dots, M - 1$; and 0 if $m = M$.

The variance σ_η^2 was set such that about 15% of the measurements contain errors. Fig. 2 shows the true and estimated

maps for a particular realization of sensor locations $\{\mathbf{x}_n\}$ (represented by the crosses) and measurement vectors $\{\phi_p(\mathbf{x}_n)\}$ and measurement noise $\eta_p(\mathbf{x}_n)$. Each sensor reports $P = 8$ measurements quantized to $b = 5$ bits. Although every sensor transmits only 5 bytes, it is observed that the reconstructed PSD maps match well with the true ones for all sources.

To quantify the estimation performance, the normalized mean-square error (NMSE), defined as

$$\text{NMSE} := \frac{\mathbb{E}\{\|\mathbf{l}(\mathbf{x}) - \hat{\mathbf{l}}(\mathbf{x})\|_2^2\}}{\mathbb{E}\{\|\mathbf{l}(\mathbf{x})\|_2^2\}} \quad (40)$$

was employed, where the expectation is taken with respect to the uniformly distributed \mathbf{x} . The region of interest was the one-dimensional ($d = 1$) interval $[0, 1] \subset \mathbb{R}^1$, and $M - 1 = 4$ sources with parameters $x_1 = 0.1$, $x_2 = 0.2$, $x_3 = 0.4$, $x_4 = 0.8$, $A_1 = 0.8$, $A_2 = 0.9$, $A_3 = 0.8$ and $A_4 = 0.7$, were considered.

To illustrate the effects of quantization on the map estimation performance, Fig. 3 depicts the NMSE as a function of N for different values of b using both nonparametric and semiparametric estimators. To capture only quantization effects, no measurement errors were introduced ($\sigma_\eta^2 = 0$), uniform quantization was used, and σ_s^2 was set to zero. The nonparametric approach was tested using a diagonal Gaussian kernel (GK) as in Fig. 2. It can be seen that the proposed estimators are consistent in N . For this particular case, it is observed that TPS outperforms GK-based regression, although this should be dependent on the choice of kernels and their parameters, as well as the field characteristics.

Fig. 4 depicts the NMSE for $N = 40$ sensors with a varying number of measurements P per sensor in different settings. First, it is seen that the estimates are inconsistent as P grows. Since the number of sensors is fixed, the field can be accurately

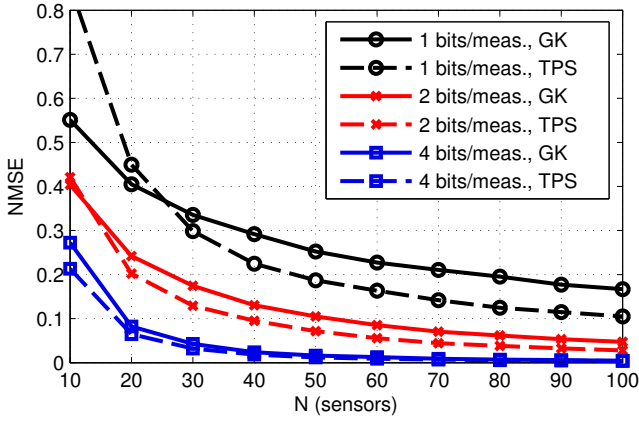


Fig. 3: NMSE versus N for variable UQ resolution with $M = 5$, $P = 5$, $\sigma_\eta^2 = 0$, $\lambda = 10^{-6}$, and nonnegativity not enforced.

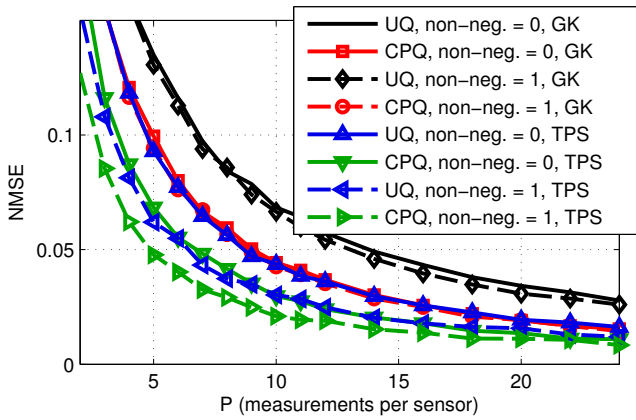


Fig. 4: Performance of different quantizers with and without nonnegativity constraints ($M = 5$, $N = 40$, $b = 2$ bits/measurement, $\sigma_\eta^2 = 0$, and $\lambda = 10^{-6}$).

estimated only in the vicinity of the sensors. It is also seen that TPS regression benefits more from incorporating non-negativity constraints than the GK-based schemes. Finally, it is observed that CPQ outperforms UQ. However, as it can be deduced from Fig. 5, this is not the case when the measurement noise variance σ_η^2 is large. This suggests that CPQ may be suboptimum under large measurement errors. Fig. 5 further shows that the effect of measurement noise is more pronounced for larger b . This is intuitive since a given measurement noise variance leads to more measurement error events. Thus, $\pi_p(x_n)$ must be estimated more accurately under finer quantization.

Fig. 6 depicts the performance of the online algorithm using the representation in (37). The offline (batch) algorithm was run per time slot with all the data received up to that time slot. The top panel in Fig. 6 shows the regularized empirical risks (evaluated per time slot using the entire set of observations) for different learning rates μ_t . Common to gradient methods with constant step size, a larger μ_t speeds up convergence, but also increases the residual error. The bottom panel depicts the NMSE evolution over time. Using the NMSE as figure of merit, favors greater learning rates over smaller ones.

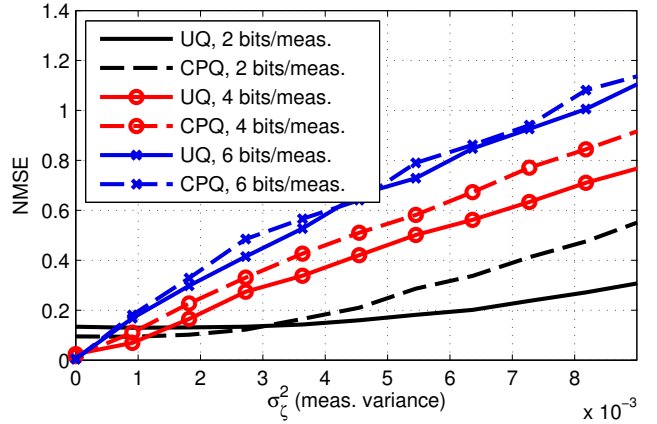


Fig. 5: Measurement noise effects ($M = 5$, $N = 40$, $P = 5$, $\lambda = 10^{-6}$, GK, and nonnegativity not enforced).

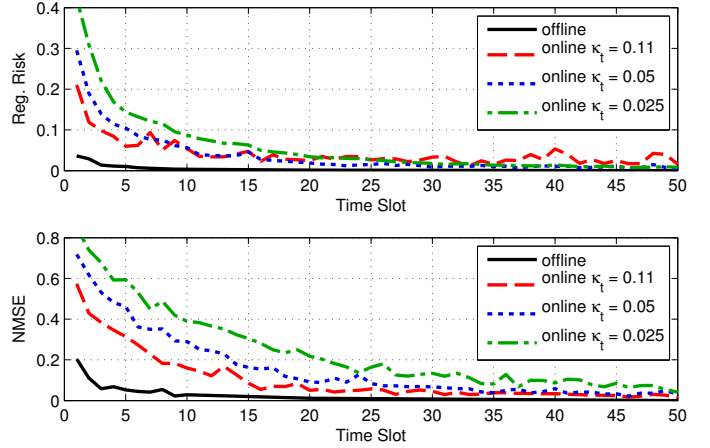


Fig. 6: Performance of the online algorithm ($M = 5$, $N = 30$, $b = 4$ bits/measurement, $\sigma_\eta^2 = 0$, $\lambda = 10^{-6}$, GK, and nonnegativity not enforced).

VI. CONCLUSIONS

This paper introduced a family of methods for nonparametric and semiparametric estimation of spatial fields using a set of linearly compressed power measurements collected by distributed sensors. The estimation task is cast in an RKHS framework that subsumes nonparametric vector SVMs. Existing semiparametric regression techniques were generalized to vector-valued function estimation. Thin-plate spline regression was seen to be a special case. Extensions to multiple measurements per sensor, non-uniform quantization and non-negativity constraints were also introduced. Batch and online approaches were developed, thus offering a performance complexity trade-off.

Future work will be devoted to kernel selection [16], quantizer design, and alternative types of spectral cartography formats including construction of channel gain maps.

APPENDIX A
DERIVATION OF (22)

This appendix describes how to obtain \hat{c} and $\hat{\theta}$ in (20) from $(\hat{\alpha}, \hat{\beta})$ in (21). Because of the change of variable, (21) is not the dual of (20); as a result \hat{c} and $\hat{\theta}$ are not, in general, the Lagrange multipliers of (21). As shown next, they can be recovered after relating (21) to the dual of (20). The latter is given by

$$\begin{aligned} (\check{c}, \check{\alpha}, \check{\beta}) &\in \arg \min_{\check{c}, \check{\alpha}, \check{\beta}} \lambda N \check{c}^T P_B^\perp K' P_B^\perp \check{c} \\ &\quad - (\mathbf{y} - \epsilon \mathbf{1}_N)^T \check{\alpha} + (\mathbf{y} + \epsilon \mathbf{1}_N)^T \check{\beta} \\ \text{s. to } &2\lambda N P_B^\perp K' P_B^\perp \check{c} - P_B^\perp K' \Phi_0 (\check{\alpha} - \check{\beta}) = \mathbf{0}_{MN} \\ &B^T \Phi_0 (\check{\alpha} - \check{\beta}) = \mathbf{0}_{MN_B} \\ &\check{\alpha} - \mathbf{1}_N \leq \mathbf{0}_N, -\check{\alpha} \leq \mathbf{0}_N, \check{\beta} - \mathbf{1}_N \leq \mathbf{0}_N, -\check{\beta} \leq \mathbf{0}_N. \end{aligned} \quad (41)$$

The presence of \check{c} in both (20) and (41) is owing to the fact that $P_B^\perp K' P_B^\perp$ is not invertible. Taking into account that (20) is indeed the dual of (41), it can be shown that $\hat{\theta}$ is the Lagrange multiplier $\check{\mu}_2$ associated with the second equality constraint of (41), whereas $\hat{c} = \check{c}$. Thus, it remains only to express $\check{\mu}_2$ and \check{c} in terms of the solution of (21).

From the second equality constraint in (41), it holds for $(\check{\alpha}, \check{\beta})$ feasible that $\Phi_0 (\check{\alpha} - \check{\beta}) = P_B^\perp \Phi_0 (\check{\alpha} - \check{\beta})$. Then, the first equality constraint in (41) can be replaced with

$$2\lambda N P_B^\perp K' P_B^\perp \check{c} - P_B^\perp K' P_B^\perp \Phi_0 (\check{\alpha} - \check{\beta}) = \mathbf{0}_{MN}. \quad (42)$$

Solving (42) for \check{c} produces

$$\check{c} = \frac{1}{2\lambda N} \Phi_0 (\check{\alpha} - \check{\beta}) + \nu(P_B^\perp K' P_B^\perp) \quad (43)$$

where $\nu(A)$ denotes any vector in the null space of A . Substituting (43) into (41), one recovers (21).

Clearly, problems (41) and (21) are equivalent in the sense that if $(\hat{\alpha}, \hat{\beta})$ solves the latter, then

$$\check{c} = \frac{1}{2\lambda N} \Phi_0 (\hat{\alpha} - \hat{\beta}), \quad \check{\alpha} = \hat{\alpha}, \quad \check{\beta} = \hat{\beta} \quad (44)$$

solve the former. However, their Lagrange multipliers differ due to the transformation introduced. A possible means of establishing their relation is to compare the KKT conditions of both problems. In particular, let $\hat{\mu}_2, \hat{\nu}_1, \hat{\nu}_2, \hat{\nu}_3, \hat{\nu}_4$ denote the Lagrange multipliers corresponding to $(\hat{\alpha}, \hat{\beta})$, associated with the constraints of (21) in the same order listed here; then the multipliers

$$\begin{aligned} \check{\mu}_1 &= -\check{c}, \quad \check{\mu}_2 = \hat{\mu}_2 - (B^T B)^{-1} B^T K' \check{c}, \\ \check{\nu}_1 &= \hat{\nu}_1, \quad \check{\nu}_2 = \hat{\nu}_2, \quad \check{\nu}_3 = \hat{\nu}_3, \quad \check{\nu}_4 = \hat{\nu}_4 \end{aligned} \quad (45)$$

correspond to the solution of (41) given by (44). Recalling that $\hat{\theta} = \hat{\mu}_2$ one readily arrives at (22).

APPENDIX B
EFFICIENT IMPLEMENTATION OF A SPECIAL CASE

In practice, one may effectively ignore the dependencies between the entries $l_m(x)$, $m = 1, \dots, M$, by using a diagonal kernel $K(x, x')$ and diagonal basis functions $B_\nu(x)$. Furthermore, one may be interested in modeling all entries

identically, as in TPS regression. Then, both the kernel and basis functions become scaled identity matrices; that is, for certain scalar functions $K(x, x')$ and $B_\nu(x)$, one has

$$K(x, x') := K(x, x') I_M \quad (46)$$

$$B_\nu(x) := B_\nu(x) I_M, \quad \nu = 1, \dots, N_B. \quad (47)$$

Thus, upon defining $\check{K} \in \mathbb{R}^{N \times N}$ with (n, n') -entry equal to $K(x_n, x_{n'})$, and $\check{B} \in \mathbb{R}^{N \times N_B}$ with (n, ν) -entry equal to $B_\nu(x_n)$, matrices K and B can be written as

$$K = \check{K} \otimes I_M \quad (48)$$

$$B = \check{B} \otimes I_M. \quad (49)$$

Then, the computation of certain matrices involved in the proposed algorithms can be done efficiently as described next.

Start by constructing a selection matrix S containing ones and zeros such that $A \odot B = (A \otimes B)S$, and define $\bar{\Phi}_0 := (I_N \otimes \mathbf{1}_P^T) \odot \bar{\Phi}$ (c.f. Sec. III-D) and (48) to obtain

$$\begin{aligned} \bar{\Phi}_0^T K &= [(I_N \otimes \mathbf{1}_P^T) \odot \bar{\Phi}]^T (\check{K} \otimes I_M) \\ &= S^T [(I_N \otimes \mathbf{1}_P) \otimes \bar{\Phi}^T] (\check{K} \otimes I_M) \\ &= S^T [(I_N \otimes \mathbf{1}_P) \check{K} \otimes \bar{\Phi}^T] \\ &= S^T [(\check{K} \otimes \mathbf{1}_P) \otimes \bar{\Phi}^T] \\ &= [(\check{K} \otimes \mathbf{1}_P^T) \odot \bar{\Phi}]^T. \end{aligned} \quad (50)$$

Likewise, one can verify that

$$\bar{\Phi}_0^T B = [(\check{B}^T \otimes \mathbf{1}_P^T) \odot \bar{\Phi}]^T. \quad (51)$$

Using the Kronecker product properties, P_B^\perp can be written as

$$\begin{aligned} P_B^\perp &= I_{MN} - (\check{B}(\check{B}^T \check{B})^{-1} \check{B}^T) \otimes I_M \\ &= (I_N - \check{B}(\check{B}^T \check{B})^{-1} \check{B}^T) \otimes I_M = P_B^\perp \otimes I_M \end{aligned} \quad (52)$$

where $P_B^\perp := I_N - \check{B}(\check{B}^T \check{B})^{-1} \check{B}^T$. Also, from (29)

$$\begin{aligned} \check{K} &= \bar{\Phi}_0^T (P_B^\perp \otimes I_M) (\check{K} \otimes I_M) (P_B^\perp \otimes I_M) \bar{\Phi}_0 \\ &= \bar{\Phi}_0^T (P_B^\perp \check{K} P_B^\perp \otimes I_M) \bar{\Phi}_0 \\ &= ((I_N \otimes \mathbf{1}_P^T) \odot \bar{\Phi})^T (P_B^\perp \check{K} P_B^\perp \otimes I_M) \cdot ((I_N \otimes \mathbf{1}_P^T) \odot \bar{\Phi}) \\ &= S^T ((I_N \otimes \mathbf{1}_P^T) \otimes \bar{\Phi})^T (P_B^\perp \check{K} P_B^\perp \otimes I_M) \\ &\quad \cdot ((I_N \otimes \mathbf{1}_P^T) \otimes \bar{\Phi}) S \\ &= S^T [(I_N \otimes \mathbf{1}_P) P_B^\perp \check{K} P_B^\perp (I_N \otimes \mathbf{1}_P^T) \otimes \bar{\Phi}^T \bar{\Phi}] S \\ &= (I_N \otimes \mathbf{1}_P) P_B^\perp \check{K} P_B^\perp (I_N \otimes \mathbf{1}_P^T) \odot \bar{\Phi}^T \bar{\Phi} \\ &= (P_B^\perp \check{K} P_B^\perp \otimes \mathbf{1}_P \mathbf{1}_P^T) \odot \bar{\Phi}^T \bar{\Phi}. \end{aligned} \quad (53)$$

Finally, θ can be obtained as (cf. Sec. III-D):

$$\theta = \bar{\mu} - [(\check{B}^T \check{B})^{-1} \check{B}^T \check{K} \otimes I_M] \hat{c}. \quad (54)$$

APPENDIX C
PROOF OF THEOREM 1

The following proof extends that of [4, Thm. 1] which cannot accommodate the instantaneous cost from (30) when $\mathcal{L} = \mathcal{L}_{1\epsilon}$ since $\mathcal{L}_{1\epsilon}$ is not differentiable and $\phi(x_\nu)$ is not constant over ν .

Expanding the norms into inner products and employing (31), one finds that

$$\begin{aligned}
& \|\mathbf{l}^{(t)} - \mathbf{g}\|_{\mathcal{H}}^2 - \|\mathbf{l}^{(t+1)} - \mathbf{g}\|_{\mathcal{H}}^2 \\
&= -\|\mathbf{l}^{(t+1)} - \mathbf{l}^{(t)}\|_{\mathcal{H}}^2 - 2\langle \mathbf{l}^{(t+1)} - \mathbf{l}^{(t)}, \mathbf{l}^{(t)} - \mathbf{g} \rangle_{\mathcal{H}} \\
&= -\mu_t^2 \|\partial_t \mathcal{C}(\mathbf{l}^{(t)}, \phi(\mathbf{x}_{n_t}), \mathbf{x}_{n_t}, y(\mathbf{x}_{n_t}))\|_{\mathcal{H}}^2 \\
&\quad + 2\langle \mu_t \partial_t \mathcal{C}(\mathbf{l}^{(t)}, \phi(\mathbf{x}_{n_t}), \mathbf{x}_{n_t}, y(\mathbf{x}_{n_t})), \mathbf{l}^{(t)} - \mathbf{g} \rangle_{\mathcal{H}}.
\end{aligned} \tag{55}$$

To bound the norm in (55), apply the triangle inequality to (32) to obtain:

$$\begin{aligned}
& \|\partial_t \mathcal{C}(\mathbf{l}, \phi(\mathbf{x}_\nu), \mathbf{x}_\nu, y(\mathbf{x}_\nu))\|_{\mathcal{H}} \\
&\leq |\mathcal{L}'_{1\epsilon}(y(\mathbf{x}_\nu) - \phi^T(\mathbf{x}_\nu)\mathbf{l}(\mathbf{x}_\nu))| \|\mathbf{K}(\cdot, \mathbf{x}_\nu)\phi(\mathbf{x}_\nu)\|_{\mathcal{H}} + 2\lambda\|\mathbf{l}\|_{\mathcal{H}}.
\end{aligned}$$

Since $\mathcal{L}_{1\epsilon}$ is 1-Lipschitz, $\mathcal{L}'_{1\epsilon}(e) \leq 1 \forall e$. Moreover, the reproducing property (cf. Sec. III-A) implies that $\|\mathbf{K}(\cdot, \mathbf{x}_\nu)\phi(\mathbf{x}_\nu)\|_{\mathcal{H}} = (\phi^T(\mathbf{x}_\nu)\mathbf{K}(\mathbf{x}_\nu, \mathbf{x}_\nu)\phi(\mathbf{x}_\nu))^{1/2} < \bar{\lambda}\|\phi(\mathbf{x}_\nu)\|$, and hence

$$\|\partial_t \mathcal{C}(\mathbf{l}, \phi(\mathbf{x}_\nu), \mathbf{x}_\nu, y(\mathbf{x}_\nu))\|_{\mathcal{H}} \leq \bar{\lambda}\|\phi(\mathbf{x}_\nu)\| + 2\lambda\|\mathbf{l}\|_{\mathcal{H}}. \tag{56}$$

Similarly, from (34) and the triangular inequality, one finds that

$$\|\mathbf{l}^{(t+1)}\|_{\mathcal{H}} \leq (1 - 2\mu_t\bar{\lambda})\|\mathbf{l}^{(t)}\|_{\mathcal{H}} + \mu_t\bar{\lambda}\|\phi(\mathbf{x}_\nu)\|.$$

Recalling that $\mathbf{l}^{(1)} = \mathbf{0}$, it is simple to show by induction that $\|\mathbf{l}^{(t)}\|_{\mathcal{H}} \leq U := \bar{\lambda}\bar{\varphi}/2\lambda$ for all t . This fact and $\|\phi(\mathbf{x}_{n_t})\|_2 \leq \bar{\varphi}$ applied to (56) produce

$$\|\partial_t \mathcal{C}(\mathbf{l}, \phi(\mathbf{x}_\nu), \mathbf{x}_\nu, y(\mathbf{x}_\nu))\|_{\mathcal{H}} \leq \bar{\lambda}\bar{\varphi} + 2\lambda U = 2\bar{\lambda}\bar{\varphi}. \tag{57}$$

for all \mathbf{l} . On the other hand, the last term in (55) can be bounded by invoking the definition of subgradient:

$$\begin{aligned}
& \langle \partial_t \mathcal{C}(\mathbf{l}^{(t)}, \phi(\mathbf{x}_{n_t}), \mathbf{x}_{n_t}, y(\mathbf{x}_{n_t})), \mathbf{l}^{(t)} - \mathbf{g} \rangle_{\mathcal{H}} \\
&\geq \mathcal{C}(\mathbf{l}^{(t)}, \phi(\mathbf{x}_{n_t}), \mathbf{x}_{n_t}, y(\mathbf{x}_{n_t})) - \mathcal{C}(\mathbf{g}, \phi(\mathbf{x}_{n_t}), \mathbf{x}_{n_t}, y(\mathbf{x}_{n_t})).
\end{aligned} \tag{58}$$

Combining (57) and (58) with (55) results in

$$\begin{aligned}
& \|\mathbf{l}^{(t)} - \mathbf{g}\|_{\mathcal{H}}^2 - \|\mathbf{l}^{(t+1)} - \mathbf{g}\|_{\mathcal{H}}^2 \\
&\geq -4\mu_t^2\bar{\lambda}^2\bar{\varphi}^2 - 2\mu_t[\mathcal{C}(\mathbf{g}, \phi(\mathbf{x}_{n_t}), \mathbf{x}_{n_t}, y(\mathbf{x}_{n_t})) \\
&\quad - \mathcal{C}(\mathbf{l}^{(t)}, \phi(\mathbf{x}_{n_t}), \mathbf{x}_{n_t}, y(\mathbf{x}_{n_t}))].
\end{aligned}$$

Adapting the proof of [4, Prop. 3.1(iii)], it can be shown that if $\mathbf{g} \in \mathcal{H}$ equals the value of \mathbf{l} attaining the infimum on the right hand side of (38), then $\|\mathbf{g}\|_{\mathcal{H}} \leq U$. For such a \mathbf{g} one has

$$\frac{1}{\mu_t}\|\mathbf{l}^{(t)} - \mathbf{g}\|_{\mathcal{H}}^2 - \frac{1}{\mu_{t+1}}\|\mathbf{l}^{(t+1)} - \mathbf{g}\|_{\mathcal{H}}^2 \tag{59}$$

$$= \frac{1}{\mu_t} \left[\|\mathbf{l}^{(t)} - \mathbf{g}\|_{\mathcal{H}}^2 - \|\mathbf{l}^{(t+1)} - \mathbf{g}\|_{\mathcal{H}}^2 \right] \tag{60}$$

$$- \left(\frac{1}{\mu_{t+1}} - \frac{1}{\mu_t} \right) \|\mathbf{l}^{(t+1)} - \mathbf{g}\|_{\mathcal{H}}^2 \tag{61}$$

$$\begin{aligned}
& \geq -4\mu_t\bar{\lambda}^2\bar{\varphi}^2 - 2[\mathcal{C}(\mathbf{g}, \phi(\mathbf{x}_{n_t}), \mathbf{x}_{n_t}, y(\mathbf{x}_{n_t})) \\
&\quad - \mathcal{C}(\mathbf{l}^{(t)}, \phi(\mathbf{x}_{n_t}), \mathbf{x}_{n_t}, y(\mathbf{x}_{n_t}))] + \left(\frac{1}{\mu_t} - \frac{1}{\mu_{t+1}} \right) 4U^2 \tag{62}
\end{aligned}$$

since $\|\mathbf{l}^{(t+1)} - \mathbf{g}\|_{\mathcal{H}} \leq 2U$. Summing for $t = 1, \dots, T$ and applying $\sum_{t=1}^T \mu_t \leq 2\mu\sqrt{T}$ [24] together with $\sqrt{T+1} - 1 \leq \sqrt{T}$ the result in (38) follows readily.

REFERENCES

- [1] A. Alaya-Feki, S. B. Jemaa, B. Sayrac, P. Houze, and E. Moulines, "Informed spectrum usage in cognitive radio networks: Interference cartography," in *Proc. IEEE Int. Symp. Personal, Indoor Mobile Radio Commun.*, 2008, pp. 1–5.
- [2] A. Argyriou and F. Dinuzzo, "A unifying view of representer theorems," in *Proc. Int. Conf. Mach. Learning*, Beijing, China, Jun. 2014.
- [3] D. D. Ariananda, D. Romero, and G. Leus, "Cooperative compressive power spectrum estimation," in *Proc. of IEEE Sensor Array Multichannel Sig. Process. Workshop*, A Corunha, Spain, Jun. 2014, pp. 97–100.
- [4] J. Audiffren and H. Kadri, "Online learning with multiple operator-valued kernels," Preprint at <http://arXiv.org/abs/1311.0222>, 2013.
- [5] E. Axell, G. Leus, E. G. Larsson, and H. V. Poor, "Spectrum sensing for cognitive radio: State-of-the-art and recent advances," *IEEE Sig. Process. Mag.*, vol. 29, no. 3, pp. 101–116, May 2012.
- [6] J.-A. Bazerque and G. B. Giannakis, "Distributed spectrum sensing for cognitive radio networks by exploiting sparsity," *IEEE Trans. Sig. Process.*, vol. 58, no. 3, pp. 1847–1862, Mar. 2010.
- [7] —, "Nonparametric basis pursuit via kernel-based learning," *IEEE Sig. Process. Mag.*, vol. 28, no. 30, pp. 112–125, 2013.
- [8] J.-A. Bazerque, G. Mateos, and G. B. Giannakis, "Group-lasso on splines for spectrum cartography," *IEEE Trans. Sig. Process.*, vol. 59, no. 10, pp. 4648–4663, Oct. 2011.
- [9] A. Berlinet and C. Thomas-Agnan, *Reproducing Kernel Hilbert Spaces in Probability and Statistics*. Springer, 2004.
- [10] F. L. Bookstein, "Principal warps: Thin-plate splines and the decomposition of deformations," *IEEE Trans. Pattern Anal. Mach. Intel.*, vol. 11, no. 6, pp. 567–585, 1989.
- [11] C. Carmeli, E. De Vito, A. Toigo, and V. Umanita, "Vector valued reproducing kernel Hilbert spaces and universality," *Analysis Appl.*, vol. 8, no. 1, pp. 19–61, 2010.
- [12] E. Dall'Anese, S.-J. Kim, G. B. Giannakis, and S. Pupolin, "Power control for cognitive radio networks under channel uncertainty," *IEEE Trans. Wireless Commun.*, vol. 10, no. 10, pp. 3541–3551, 2011.
- [13] E. Dall'Anese, J.-A. Bazerque, and G. B. Giannakis, "Group sparse lasso for cognitive network sensing robust to model uncertainties and outliers," *Phys. Commun.*, vol. 5, no. 2, pp. 161–172, 2012.
- [14] T. Diethe and M. Girolami, "Online learning with (multiple) kernels: A review," *Neural Comput.*, vol. 25, no. 3, pp. 567–625, Mar. 2013.
- [15] G. Ding, J. Wang, Q. Wu, Y. Yao, F. Song, and T. A. Tsiftsis, "Cellular-base-station-assisted device-to-device communications in TV white space," *IEEE J. Sel. Areas Commun.*, vol. 34, no. 1, pp. 107–121, Jan. 2016.
- [16] M. Gönen and E. Alpaydm, "Multiple kernel learning algorithms," *J. Mach. Learn. Res.*, vol. 12, pp. 2211–2268, 2011.
- [17] M. Gudmundson, "Correlation model for shadow fading in mobile radio systems," *Electron. Letters*, vol. 27, no. 23, pp. 2145–2146, 1991.
- [18] D.-H. Huang, S.-H. Wu, W.-R. Wu, and P.-H. Wang, "Cooperative radio source positioning and power map reconstruction: A sparse Bayesian learning approach," *IEEE Trans. Veh. Technol.*, vol. 64, no. 6, pp. 2318–2332, Jun. 2015.
- [19] B. A. Jayawickrama, E. Dutkiewicz, I. Oppermann, G. Fang, and J. Ding, "Improved performance of spectrum cartography based on compressive sensing in cognitive radio networks," in *Proc. Int. Conf. Commun.*, Budapest, Hungary, Jun. 2013, pp. 5657–5661.
- [20] V. Kecman, M. Vogt, and T. M. Huang, "On the equality of kernel AdaTron and sequential minimal optimization in classification and regression tasks and alike algorithms for kernel machines," in *Proc. European Symp. Artificial Neural Netw.*, Bruges, Belgium, Apr. 2003, pp. 215–222.
- [21] S.-J. Kim, E. Dall'Anese, and G. B. Giannakis, "Cooperative spectrum sensing for cognitive radios using kriged Kalman filtering," *IEEE J. Sel. Topics Sig. Process.*, vol. 5, no. 1, pp. 24–36, Feb 2011.
- [22] S.-J. Kim and G. B. Giannakis, "Cognitive radio spectrum prediction using dictionary learning," in *Proc. IEEE Global Commun. Conf.*, Atlanta, GA, Dec. 2013.
- [23] S.-J. Kim, N. Jain, G. B. Giannakis, and P. Forero, "Joint link learning and cognitive radio sensing," in *Proc. Asilomar Conf. Sig., Syst., Comput.*, Pacific Grove, CA, Nov. 2011.
- [24] J. Kivinen, A. J. Smola, and R. C. Williamson, "Online learning with kernels," *IEEE Trans. Sig. Process.*, vol. 52, no. 8, pp. 2165–2176, 2004.
- [25] O. Mehanha and N. Sidiropoulos, "Frugal sensing: Wideband power spectrum sensing from few bits," *IEEE Trans. Sig. Process.*, vol. 61, no. 10, pp. 2693–2703, May 2013.
- [26] C. A. Micchelli and M. Pontil, "On learning vector-valued functions," *Neural Comput.*, vol. 17, no. 1, pp. 177–204, 2005.

- [27] J. C. Platt, "Fast training of support vector machines using sequential minimal optimization," in *Advances in Kernel Methods*. Cambridge, MA: MIT Press, 1999, pp. 185–208.
- [28] Z. Quan, S. Cui, H. Poor, and A. Sayed, "Collaborative wideband sensing for cognitive radios," *IEEE Sig. Process. Mag.*, vol. 25, no. 6, pp. 60–73, 2008.
- [29] A. Ribeiro and G. B. Giannakis, "Bandwidth-constrained distributed estimation for wireless sensor networks: Part I/II," *IEEE Trans. Sig. Process.*, vol. 54, no. 3/7, pp. 1131–1143/2784–2796, 2006.
- [30] D. Romero and G. Leus, "Wideband spectrum sensing from compressed measurements using spectral prior information," *IEEE Trans. Sig. Process.*, vol. 61, no. 24, pp. 6232–6246, 2013.
- [31] B. Schölkopf and A. J. Smola, *Learning with Kernels: Support Vector Machines, Regularization, Optimization, and Beyond*. MIT Press, 2002.
- [32] D. J. Sebald and J. A. Bucklew, "Support vector machine techniques for nonlinear equalization," *IEEE Trans. Sig. Process.*, vol. 48, no. 11, pp. 3217–3226, 2000.
- [33] A. J. Smola and B. Schölkopf, "A tutorial on support vector regression," *Stat. Comput.*, vol. 14, no. 3, pp. 199–222, 2004.
- [34] A. J. Smola, B. Schölkopf, and K.-R. Müller, "The connection between regularization operators and support vector kernels," *Neural Netw.*, vol. 11, no. 4, pp. 637–649, 1998.
- [35] R. Tandra and A. Sahai, "SNR walls for signal detection," *IEEE J. Sel. Topics Sig. Process.*, vol. 2, no. 1, pp. 4–17, 2008.
- [36] J. A. Tropp, J. N. Laska, M. F. Duarte, J. K. Romberg, and R. G. Baraniuk, "Beyond Nyquist: Efficient sampling of sparse bandlimited signals," *IEEE Trans. Inf. Theory*, vol. 56, no. 1, pp. 520–544, Jan. 2010.
- [37] G. Vázquez-Vilar and R. López-Valcarce, "Spectrum sensing exploiting guard bands and weak channels," *IEEE Trans. Sig. Process.*, vol. 59, no. 12, pp. 6045–6057, 2011.
- [38] G. Wahba, *Spline Models for Observational Data*, ser. CBMS-NSF Regional Conference Series in Applied Mathematics. SIAM, 1990, vol. 59.
- [39] S. Wang, W. Zhu, and Z.-P. Liang, "Shape deformation: SVM regression and application to medical image segmentation," in *Proc. Int. Conf. Comput. Vis.*, vol. 2, Vancouver, Canada, 2001, pp. 209–216.
- [40] Z. Wang, K. Crammer, and S. Vucetic, "Breaking the curse of kernelization: Budgeted stochastic gradient descent for large-scale svm training," *J. Machine Learning Research*, vol. 13, no. 1, pp. 3103–3131, 2012.
- [41] T. Yucek and H. Arslan, "A survey of spectrum sensing algorithms for cognitive radio applications," *IEEE Commun. Surveys Tutorials*, vol. 11, no. 1, pp. 116–130, 2009.